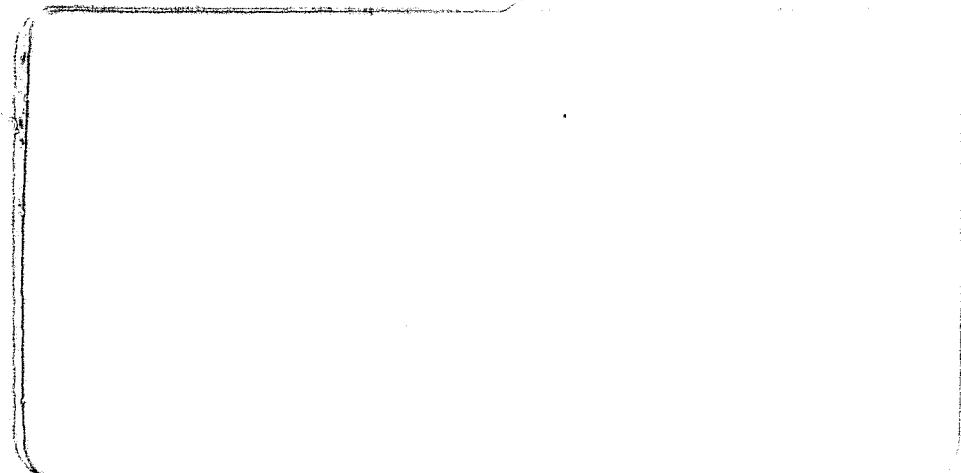**General Disclaimer**

One or more of the Following Statements may affect this Document

- This document has been reproduced from the best copy furnished by the organizational source. It is being released in the interest of making available as much information as possible.

- This document may contain data, which exceeds the sheet parameters. It was furnished in this condition by the organizational source and is the best copy available.

- This document may contain tone-on-tone or color graphs, charts and/or pictures, which have been reproduced in black and white.

- This document is paginated as submitted by the original source.

- Portions of this document are not fully legible due to the historical nature of some of the material. However, it is the best reproduction available from the original submission.
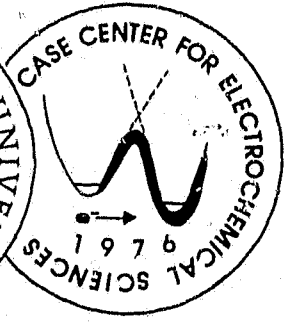
CASE CENTER FOR
ELECTROCHEMICAL SCIENCES

CASE INSTITUTE OF TECHNOLOGY
CASE WESTERN RESERVE UNIVERSITY
UNIVERSITY CIRCLE   CLEVELAND, OHIO 44106

ELECTROCHEMICAL STUDIES OF REDOX SYSTEMS

FOR ENERGY STORAGE

Semi-Annual Report III
4 December 1982 - 31 May 1983

NASA-Lewis Project   NAG 3-219

by

Cherng-Dean Wu
Ernesto Julio Calvo
Ernest Yeager

Case Center for Electrochemical Sciences
and The Chemistry Department
Case Western Reserve University
Cleveland, Ohio 44106

September 30, 1983

TABLE OF CONTENTS

SUMMARY OF REPORT

During the past six months attention has been focused on a quantitative understanding of several experimental results presented qualitatively in the last semi-annual report. Furthermore, some new experiments have been carried out and analyzed.

Particular attention has been paid to the Cr(II)/Cr(III) redox couple in aqueous solutions in the presence of Cl^- ions. The aim of this research has been to unravel the electrode kinetics of this redox couple and the effect of Cl^- and electrode substrate. Gold and silver have been studied as electrodes and the results show distinctive differences; this is probably due to the role Cl^- ion may play as a mediator in the reaction and the difference in state of electrical charge on these two metals (difference in the potential of zero charge, pzc).

To prove this point, future experiments are planned with the basal plane of stress annealed pyrolytic graphite. On this low defective surface, anions are not significantly adsorbed and therefore this will provide a good test for the role of Cl^-.

The competition of hydrogen evolution with $CrCl_3$ reduction on these surfaces has been studied by means of the rotating ring-disk electrode (RRDE). The ring downstream measures the flux of chromous ions from the disk and therefore separation of both Cr(III) and H_2 generation can be achieved by analyzing ring and disk currents. The conditions for the quantitative detection of Cr^{2+} at the ring electrode have been established.

Underpotential deposition of Pb on Ag and its effect on the electrokinetics of Cr(II)/Cr(III) reaction have been studied. The rationale behind the use of these upd layers has been to suppress the hydrogen

evolution and to modify the electronic properties of the electrode surface where the electro-reduction of $CrCl_3$ takes place. On silver the hydrogen over-voltage is large enough for the $CrCl_3$ reaction to be observed at the convective-diffusion potential regime.

As it has been reported for gold substrate, the underpotential deposition of lead on silver also produces a hindrance of the $Cr(III)/Cr(II)$ redox couple kinetics. Models for the inhibition effect are presented from a phenomenological knowledge of Pb upd on polycrystalline silver.

I. OBJECTIVES OF RESEARCH

Energy storage systems based on redox couples in which both the oxidized and reduced species exist in solution have several advantages over conventional batteries when used for load-leveling and for solar/ wind energy storage. The principal advantages are very good cycle life and long term reliability plus reasonable cost and minimal environmental impact.

NASA-Lewis has developed an effective redox electrochemical system for energy storage. This system is based on an electrochemical cell with two compartments separated by an ion selective membrane. The electrode reaction at the negative electrode involves the chromous/chromic redox couple while that at the positive electrode involves the ferrous/ferric redox couple. Solutions containing these species are circulated through carbon felt electrodes where the reduction of Cr(III) and oxidation of Fe(II) occur during charging and the reverse reactions occur during discharge.

NASA-Lewis has greatly improved the performance of the carbon electrodes used for the Cr(II)/Cr(III) reactions by incorporating gold in the

carbon felt matrix and by adding lead chloride to the solution. The resulting gold-lead catalyst greatly reduces the overpotential normally associated with this redox couple while maintaining the hydrogen over-potential sufficiently high to depress the competing hydrogen generation reaction.

While the gold-lead catalyzed carbon felt electrodes afford high performance, a full understanding of the electrochemical and other processes involved at these electrodes has not yet been achieved.

The aim of the research project is:

(a) Understanding of the role of the electrode surface through the study of single metals, alloys, underpotential deposited (UPD) metal layers, and chemically modified electrode surfaces.

(b) Understanding of the mechanisms by which various ions (particularly anions) exert rate accelerating effect on redox couples (Fe^{2+}/Fe^{3+} and Cr^{2+}/Cr^{3+}).

(c) Establishment of guidelines for the selection and optimization of specific electrode-anion-redox couple systems.

II. INTRODUCTION

The results of electrochemical studies of $CrCl_3$ reduction on gold have been reported in the first annual report (Report II). In the present report we shall deal mainly with the chromium(III)-chromium(II)-chloride system on silver electrode and compare this system with the behavior on gold electrode.

Reduction of Cr^{3+} ion in the absence of chloride in solution is negligible and only hydrogen evolution is evident on both gold and silver

electrodes. On mercury, however, due to its high hydrogen overpotential the electrokinetics of $Cr(H_2O)_6^{3+}$ reduction can be studied. This reaction takes place on a Ni(Hg) cathode at very negative potentials (ca. -1.0V vs. SCE) -- see Report II, page 9. It has been found that the presence of halide ions in the solution enhances the rates of both oxidation of Cr^{2+} and reduction of Cr^{3+} on several substrates (Hg, Au, Ag). The reason for this enhancement is to be found in several factors:

    (a) A bridging mechanism by the halide ion for the electron transfer.

    (b) Inner coordination ligand effects

    (c) Ionic double layer effects on the electrode kinetics of highly charged species.

Similar enhancement for the electrokinetics of Fe^{3+}/Fe^{2+} on Pt and Au is known to occur, but in this case the major contribution is the ionic double layer effect (1). The reaction takes place at potentials positive to the potential of zero charge (pzc) and a very low concentration of halide ion accelerates the reaction rate. For the Cr^{3+}/Cr^{2+}-Cl system it is likely that factors (a) and (b) play a major role. In order to evaluate to what extent the electrode kinetics are affected by them, the electro-reduction of $CrCl_3$ is being studied on substrates of different electronic surface properties, which are also modified by metal underpotential deposition.

III. ELECTRO-REDUCTION KINETICS OF $CrCl_3$ ON GOLD AND SILVER ELECTRODES

A. Pure Gold

On gold electrode the reaction shows three complicating features, namely:

i) time dependence

ii) current maximum

iii) hysteresis

as has been shown in Report II (Fig. 8).

These effects make the study of the electrochemistry of $CrCl_3$ on this substrate difficult. Gold also has a low hydrogen overpotential and hydrogen evolution simultaneous to the $CrCl_3$ reduction is observed. Separation of these two reactions is achieved by means of the rotating ring disk electrode (RRDE) as explained below.

Time effects for the reduction of $CrCl_3$ are illustrated in Fig. 1 for experiments carried out at different times from 30 minutes to 71 hours after a freshly prepared $CrCl_3$ solution was added to the background electrolyte under anaerobic conditions (the solution was prepared from Johnson & Mathey Puratronic chromium chloride in distilled water).

Each voltammogram in Fig. 1 was obtained under identical electrode surface conditions by polishing the gold surface with 0.05 µm alumina, and rinsing the surface before each run. The electrode was kept out of the solution between runs. Therefore the differences observed can only be related to changes in the composition of the chromium solution.

Chemical changes in solutions of $Cr(H_2O)_4Cl_2^+$ (resulting from dissolution of chromic chloride in water) are known, and are due to ligand exchange reactions (2,3).

Calculations of the relative concentrations as a function of time are explained in Appendix I and the results are shown in Fig. 2. The first-order rate constant for the aquation of the dichloro- and monochloro-complexes are very different and therefore the time scales of the processes

are widely separated. The concentration of $Cr(H_2O)_4Cl_2^+$ dies away after one hour, while $Cr(H_2O)_5Cl^{2+}$ increases to a maximum in about the same period. The decomposition of $Cr(H_2O)_5Cl^{2+}$ is much slower and a significant fraction is present in solution after several hours. Inspection of Fig. 1 and comparison with Fig. 2 show that the initial current increase and decrease for $CrCl_3$ reduction follows a similar pattern to that of the concentration of $Cr(H_2O)_5Cl^{2+}$ species in solution. This indicates that $Cr(H_2O)_5Cl^{2+}$ is the predominant electroactive species on gold electrode.

Chloride in the inner coordination sphere is therefore needed for the reduction of Cr^{3+} to occur. Aquation of the chloro-chromo complexes is slow:

$$Cr(H_2O)_4Cl_2^+ \xrightarrow{k_1} Cr(H_2O)_5Cl^{2+} + Cl^-$$
$$\xrightarrow{k_2} Cr(H_2O)_6^{3+} + Cl^-$$
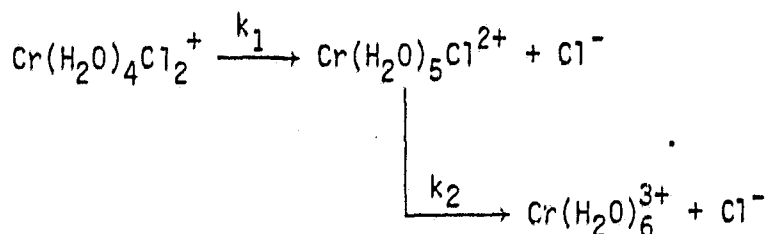
with $k_1 = 0.1 \ min^{-1}$ and $k_2 = 3.2 \times 10^{-4} \ min^{-1}$ (3). The reverse reaction

$$Cr(H_2O)_6^{3+} + Cl^- \longrightarrow Cr(H_2O)_5Cl^{2+}$$

is extremely slow. On the other hand, $Cr(H_2O)_6^{2+}$ is very labile to ligand exchange.

Evidence of aquation in the present conditions has been presented in Report II (Fig. 46) as the maxima of the visible absorption spectra shift to lower wavelength values with time. This is intepreted in terms of a decrease of chlorochromium complexes concentration and a corresponding increase in the concentration of the hexaquochromo complex (4,5). The increase in the reduction current levels at very short and decreases at

very long times indicates that $Cr(H_2O)_4Cl_2^+$ and $Cr(H_2O)_6^{3+}$ do not contribute significantly to the reduction current on gold electrode.

Another interesting feature to be noticed is that even convective-diffusion conditions are operative with the RDE, current levels of $CrCl_3$ reduction on gold are always quite below the mass transport limit (described by the Levich equation). Reproducibility of results on gold electrode is sensitive to long exposure of the electrode to the solution under the experimental conditions. This may be due to adsorption of soluble substances from the solution or slow reconstruction of the electrode surface under the experimental conditions. The maximum in Fig 1 (a, b and c) seen only at short times seems to be related to the hysteresis observed since the re-enhanced current in the reverse sweep is always lower than in the forward direction. Those maxima occur at about -0.5 V (vs. SCE) regardless of the rotation rate and it has been suggested in Report II that the effect could be due to a re-orientation of the $Cr(H_2O)_5Cl^{2+}$ complex on the gold surface.

In a cyclic voltammetric experiment it is not possible to distinguish clearly between effects due to time and potential since this is varied with time.

Fig. 3 shows potentiostatic experiments for the reduction of $CrCl_3$ on gold electrode; there is a slow decrease of the current which is more noticeable at high rotation frequencies. The steady state results have been corrected for mass transport, taking into account the mass transport limiting current 0.44 mA predicted by equation: (6)

$$i_L = 0.62 \, n \, FAD^{2/3} \, \nu^{-1/6} \, c_b \, \omega^{1/2} \tag{1}$$

with   n = 1; number of electrons per molecule involved in the

overall reaction

A = 0.2 cm^2; area of the gold disk electrode

D = 6.2 x 10^{-6} cm^2 s^{-1}; $Cr(H_2O)_5Cl^{2+}$ diffusion constant

obtained experimentally with a silver RDE electrode

on which the convective diffusion regime is observed

(see below)

$\nu \cong 0.01$ cm^2 s^{-1}; kinematic viscosity of the solvent

C_b = 4.8x10^{-6} mol cm^{-3}; total chromium concentration in

the solution

ω = 900 rpm $\equiv$ 94.2 rad s^{-1}; rotation frequency

and the plot lg $\frac{i}{i_L-i}$ vs. E is presented in Fig. 4. At low overpotentials
a Tafel slope close to 2F/RT is observed which is indicative of $\alpha \approx 0.5$ for
one-electron electrochemical rate determining step. At higher overpotentials
a current maximum is also observed in the steady state, which confirms that
this maximum at about -0.53 V is mainly due to potential rather than a
transient effect.

Since the potential range where the reduction of $CrCl_3$ occurs on gold
is negative to the potential of zero charge (pzc) (7), the adsorption of
the positvely charged species $Cr(H_2O)_5Cl^{2+}$ is expected to be favored.
Furthermore, its surface concentration is expected to increase the more
negative the electrode potential. For Langmuirian adsorption conditions:

$$\theta = (1-\theta) \; C \; exp \left(-\frac{\gamma F}{RT} \right) E \qquad\qquad (2)$$

with $-2 \leq \gamma \leq 0$, the negative sign in γ is taken to indicate that the surface concentration of positively charged species increases at negative potentials with respect to the pzc. For $\theta \ll 1$, one expects the current to increase with potential proportionally to:

$$\exp \frac{(\gamma - \alpha)F}{RT} E$$

The finding of the maximum in the steady state Tafel plot is indicative of the existence of some kinetic hindrance at about -0.5 V (SCE).

If the halide bridging mechanism is considered, the configuration of $Cr(H_2O)_5Cl^{2+}$ species on the gold electrode surface will be important in determining the rate of reduction. The configuration with the halide towards the electrode surface will have the lowest activation energy for the electron transfer process. The pentaquo-chloride chromic ion has a permanent dipolar character and therefore the number of species oriented with the chloride towards the surface will depend on the electrode potential, decreasing the more negative this is made. Thus the maximum observed could be related to a decrease in the fraction of electroactive species on the surface with the most favorable configuration for the electro-reduction process.

B. Pure Silver

On pure silver electrode only hydrogen evolution is observed when $Cr(H_2O)_6(ClO_4)_3$ is added to the background electrolyte. Addition of free Cl^- ion to this solution does not bring any significant change.

On the other hand when a freshly prepared $CrCl_3$ solution is added to the electrolyte, much larger activity for the electro-reduction than on gold is observed. Figure 6. shows that at low overpotentials larger

current is observed on gold but then the electro-reduction rate is larger on silver than gold, reaching eventually the convective-diffusion potential regime before significant contribution from hydrogen evolution is apparent.

On silver, like gold, the electro-reduction of Cr(III) proceeds with chloride in the inner coordination sphere of the complex. Unlike gold, on silver electrode no maxima or pronounced hysteresis are observed. In this respect it must be borne in mind that silver, unlike gold, is positive to its pzc under the present working conditions (7).

The higher hydrogen overpotential on silver and the absence of maxima and hysteresis make silver a better substrate for the study of the electrode kinetics of the Cr(III)/Cr(II) redox couple.

Time effects due to changes in solution composition are, however, observed similarly to gold electrode as depicted in Fig. 6. No appreciable change in the reduction curve is observed before 2 hours, then the current level decreases with time. After 42 hours, the convective-diffusion limiting current drops to 55% of its initial value which roughly corresponds to a similar decrease in the concentration of $Cr(H_2O)_5Cl^{2+}$ as it appears from Fig. 2B. However unlike gold, no initial current increase is observed on silver, which would suggest that both $Cr(H_2O)_5Cl^{2+}$ and $Cr(H_2O)_4Cl_2^{+}$ complexes might be reduced on silver. On gold, since the surface is charged negatively in respect to the solution, the lower charge and strong dipolar character would make the kinetics of $Cr(H_2O)_4Cl_2^{+}$ more difficult and only $Cr(H_2O)_5Cl^{2+}$ would be reduced.

The effect of rotation and the corresponding Levich plot for $CrCl_3$ reduction on silver are shown in Fig. 7. Good linearity and zero intercept

are found. There is not appreciable hydrogen discharge evident in the potential range studied and $CrCl_3$ reduction reaches the convective-diffusion regime.

Using the gradient of the $i_L-\omega^{1/2}$ plot in Fig. 7 and the equation: (6)

$$i_L = 0.62 \; n \; FAD^{2/3} \; \nu^{-1/6} \; \omega^{1/2} \; C_b \tag{7}$$

with
F = Faraday constant

A = Electrode area

D = Diffusion constant

ν = Kinematic viscosity

C_b = Bulk concentration

ω = Rotation rate in rad s^{-1}

for a one-electron process (n = 1) one finds $D = 6.2 \times 10^{-6}$ cm^2 s^{-1}. The diffusion constant for $Cr(H_2O)_5Cl^{2+}$ and $Cr(H_2O)_4Cl_2^+$ were not found in the literature. The diffusion constant for hexaquochromic ion has been reported to be 5.82×10^{-6} cm^2 s^{-1} at 25° C. in 0.5 M $NaClO_4$ (pH = 3) (8). In the present study, reduction of $Cr(H_2O)_6(ClO_4)_3$ on Ni amalgamated RDE has yielded $D = 1.5 \times 10^{-5}$ cm^2 s^{-1} from the data shown in Fig. 8. Since solutions made by disolving $[Cr(H_2O)_4Cl_2]Cl.2H_2O (CrCl_3)$ in water change composition with time and not all the components are necessarily active, it is difficult to know accurately C_b used in equation (1) to evaluate D. Furthermore, if both monochloro- and dichloro- complexes are active on silver electrode, an average value of their diffusion constants will be measured.

At potentials less negative to -0.7 V vs. SCE convective-diffusion kinetic coupling is observed. Then the Koutecky-Levich equation for order one process taking into account the back reaction takes the form (6):

$$\frac{1}{i} = \frac{1}{nFA(k_fC_O{}^b - k_bC_R{}^b)} \; [1 + \frac{D_O{}^{-2/3}k_f + D_R{}^{-2/3}k_b}{0.62 \; \nu^{-1/6} \; \omega^{1/2}}] \tag{3}$$

where k_f and k_b are forward and backward rate constants for

$$O + e^- \xrightleftharpoons[k_b]{k_f} R \tag{4}$$

$c_i{}^b$ is the bulk concentration of species i and the rest of the symbols have their usual meaning. In the experiments described, the concentration of the reduced species $Cr(H_2O)_6{}^{2+}$ can be regarded as negligible and therefore Equation 3 takes the form:

$$\frac{1}{i} = \frac{1}{nFAk_fC_O{}^b} \; [1 + \frac{D_O{}^{-2/3}k_f + D_R{}^{-2/3}k_b}{0.62 \; \nu^{-1/6} \; \omega^{1/2}}] \tag{5}$$

The slope of this plot, $1/i$ vs. $1/\omega^{1/2}$, is:

$$s = \frac{(k_b/k_f + 1)}{B} \tag{6}$$

with $B = 0.62 \; nFAD^{2/3} \; \nu^{-1/6} \; C_O{}^b$, assuming $D_O = D_R$.

. Fig. 9 shows $i-1$ vs. $\omega^{-1/2}$ plot corresponding to the results of Fig. 7. The change of slope with potential is indicative of the influence of the back reaction. Although this is a fast redox couple, it will be possible to study its electrokinetics with both Cr(II) and Cr(III) present in solution by means of the Randles method of analysis or transient experiments. For this aim Cr(II) must be electrogenerated _in situ_ and protected from O_2.

Silver electrodeposited from $AgNO_3$ solution on a gold substrate has also been used as electrode for the electro-reduction of $CrCl_3$. The deposition of silver has been performed ex situ by immersing the gold electrode into a 0.1 M $AgNO_3$ solution and potentiostatting the electrode at +0.5 V vs. SCE for a few minutes. The deposition occurred at the starting of bulk deposition of silver. The cathodic charge involved in the deposition was not recorded. As seen in Fig.10, the disk currents do not level off at sufficiently negative potentials and the Levich plot shows good linearity but an intercept which may be due to simultaneous H_2 evolution. The slope of the Levich plot (5.3 x 10^{-5} A $\cdot$ $s^{1/2}$) is lower than on pure silver electrode under the same conditions (ca. = 6.1 x 10^{-5} A $\cdot$ $s^{1/2}$). A linear i^{-1} - $\omega^{-1/2}$ plot (Fig. 11) shows that kinetic-diffusion coupling is still observed at -0.75 V, where pure convective-diffusion conditions prevail on silver (fig. 7).

Equation (5) predicts $1/B = 3.28$ x 10^3 A^{-1} $rad^{1/2}$ $s^{-1/2}$ with $D = 6.2$ x 10^{-6} cm^2 s^{-1}; slopes in Fig. 11 give an average value $1/B = 3.25$ x 10^3 A^{-1} $rad^{1/2}$ $s^{-1/2}$ for electrode potentials in the range -0.65 to -0.75 V.

The intercept in the i_L - $\omega^{1/2}$ plot in Fig. 10 due to simultaneous hydrogen evolution and the slower kinetics for chromic ion reduction are probably related to a heterogeneous surface with gold exposed to the solution.

Fig. 12 shows Tafel plots for $CrCl_3$ reduction on silver and silver plated gold, corrected for mass transport, where i_L stands for the limiting convective-diffusion current for $CrCl_3$ reduction on silver. Tafel slope for $CrCl_3$ reduction on silver and silver plated `d electrodes is about

2F/RT which corresponds to an electrochemical rate determining step with $\alpha \cong 0.5$ for one electron.

On gold, higher activity than on silver is observed at low overpotentials with a Tafel slope $\sim 2F/RT$ and at higher overpotentials the activity is lower than on silver, but gold shows a current maximum below the mass transport limit. This difference is probably related to differences in the surface charge in those two metals.

Although on silver plated on gold the same Tafel slope is observed as on pure silver, an intercept attributed to H_2 evolution not affected by convective-diffusion and slower kinetics than on pure silver are observed. On both gold and silver, chloride in the inner coordination sphere appears to enhance the electro-kinetics of chromic ion reduction. However, while only $Cr(H_2O)_5Cl^{2+}$ appears to be electroactive on gold, both $Cr(H_2O)_4Cl_2^{+}$ and $Cr(H_2O)_5Cl^{2+}$ seem to be reduced on silver.

C. Rotating Ring Disk Studies of the Chromous-Chromic Couple

In order to separate simultaneous cathodic processes from the $CrCl_3$ reduction on the disk electrode, the rotating ring-disk electrode has been used. The ring electrode is potentiostatted so that the diffusional oxidation of chromium(II) ion generated a. the disk occurs. While the disk current will be generated by more than $CrCl_3$ reduction, comparison of both disk and ring currents allow separation of other cathodic process at the disk. The ring current should measure the chromium flux at the disk (9):

$$i_R = F \, N_o \, A_d \left(\frac{dc}{dx} \right)_{x=0} = 0.62 \, F \, N_o \, A_d \, D^{2/3} \, \nu^{-1/6} \, \omega^{1/2} \, c_b \qquad (7)$$

with $C^{ox}_{bulk} = C^{red}_{surface}$ and N_o the collection efficiency, is a geometric

factor of the RRDE. Calculation from geometric dimension of gold/gold RRDE (r_1 = 0.25 cm, r_2 = 0.28 cm and r_3 = 0.37 cm) gives N_0 = 0.399 (10). Experimentally this value was confirmed (N_0^{exp} = 0.398) by use of the simple redox couple Fe(II)/Fe(III) with reactions:

and

at Disk $\qquad Fe^{3+} + e^- \longrightarrow Fe^{2+}$

at Ring $\qquad Fe^{2+} \longrightarrow Fe^{3+} + e^-$

as shown in Fig. 13 for different rotation rates.

Fig. 14 shows the voltammetry on silver plated ring when the disk is making Cr(II) under potentiostatic conditions. It can be seen that the diffusional re-oxidation to Cr(III) is achieved at potentials more positive than -0.30 V. Comparison of Levich slopes for both disk and ring yields N_0 = 0.395 according to equations (1) and (7). (N_0^{theory} = 0.399)

On a gold ring, the oxidation of Cr(II) shows more complex features, as can be seen from Fig. 15. The limiting currents are below the Levich predicted convective-diffusion values (dotted line) and also time effects are observed. This suggests that similarly to what we have described for the cathodic reduction of $CrCl_3$, the electro-oxidation of Cr^{2+} ion shows complex kinetic features on gold electrode and therefore silver plated ring must be used to carry out this reaction. Qualitative preliminary results with a silver plated gold disk and a gold ring RRDE are shown in Fig. 16. Fig. 17 shows a plot of i_R vs. i_D for the results of Fig. 16, at different rotation frequencies. Good agreement with the theoretical N_0 = 0.399 is observed at low disk overpotentials. Therefore, there is not evidence of a Cr(II) titration effect in the diffusion layer, produced by residual oxygen. However at higher cathodic overpotentials, discrepancy with the

predicted ring yield is found. Since the gold ring electrode does not fulfill strictly the diffusional condition for Cr(II) oxidation, we cannot at present go further in the analysis of the present data or the competitive H_2 evolution at a silver plated gold disk. Further experiments with a silver plated ring will be carried out.

IV. LEAD UPD AND ITS EFFECT ON $CrCl_3$ REDUCTION ON SILVER ELECTRODE

A. Cyclic Voltammetry

Simultaneous underpotential deposition of lead has an inhibiting effect on the rate of $CrCl_3$ reduction on silver. This can be seen in Figure 18. From comparison of Figures a and b, one can see:

    i)   lower currents due to $CrCl_3$ reduction with simultaneous lead UPD

    ii) inversion of order, Fig. 18(b), and maximum with rotation frequency and hysteresis as compared to pure silver 18(a)

    iii) anodic lead stripping peak at about -0.40V .

The voltammetry curve in Figure 19 shows that $CrCl_3$ reduction on silver takes place in the presence of Pb(II) in solution at potentials more cathodic than the UPD of lead in the present conditions and close to the Pb/Pb^{2+} equilibrium potential.

The existence of a maximum and the decrease of current with rotation in RDE experiments indicates inhibition of the $CrCl_3$ reduction by lead simultaneously underpotential-deposited. The voltage sweeping experiments are not under well-defined conditions since the potential and time are varied simultaneously with changes in surface concentration, lead coverage and possibly lead UPD electrosorption valence during the potential sweep. From Figure 18b, one can conclude that the first part of the cyclic voltammetric scan reflects the redox couple behavior, but then the supressive effect of lead UPD becomes important and rotation affects the transport of both lead and the couple. The maximum is well below the convective-diffusion current level for $CrCl_3$ reduction. In the reverse scan, the decrease of current with rotation rate reflects the fact that

the lead coverage is still building up on the surface. The concentration of lead is sufficiently low in the bulk solution that bulk lead is never deposited onto the surface.

In order to understand the inhibition of $CrCl_3$ reduction on silver by UPD lead, the study of UPD of lead on silver in the absence of chromium in solution has been carried out. Fig. 20 shows cyclic voltammetry in which lead UPD and bulk deposition on silver with and without chloride are depicted. Chloride has an important effect on the UPD, but negligible influence in bulk deposition. In the chromium redox couple, chloride is present at a level $[Cl^-] \backsim 3[CrCl_3]$.

Consider the reaction:

$$Pb^{2+} + 2e^- \rightleftharpoons Pb(bulk) \qquad E^O_{NHE} = -0.126V \text{ at } 25°C .$$

Therefore, the Nernst potential for 0.38 mM Pb(II) is -0.474V(SCE). Taking into account the complex equilibrium:

$$Pb^{2+} + Cl^- \rightleftharpoons PbCl^+ \qquad K \backsim 20 M^{-1}$$
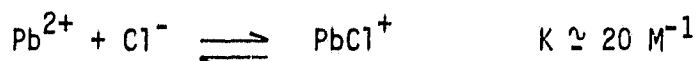
the concentration of lead ion in the presence of 3.8 mM Cl^- is

$$[Pb^{2+}] = \frac{0.38 \times 10^{-3}}{K[Cl^-]+1} = 0.35 \text{ mM}$$

and the Nernst potential -0.475V(SCE). It can be seen that chloride ion under those conditions does not appreciably modify the bulk deposition potential, and that the nucleation overpotential for bulk lead deposition is probably larger than the difference introduced by chloride.

The effect on UPD, on the other hand, is expected to be large since chloride ion adsorption will affect the UPD adsorption and probably the electrosorption valence, too. This same effect has been shown by Kolb and Gerisher [16] for lead UPD on silver(111) single crystal. Also, under the experimental conditions, $PbCl_2$ is not expected to precipitate since the ionic product $[Cl^-]^2[Pb^{2+}] < K_{sp} = 1.7 \times 10^{-5}$.

B. Potentiostatic Transients

In order to study the inhibition effect of lead on $CrCl_3$ reduction under better defined conditions, potentiostatic steps have been applied from an initial potential $E_i = -0.1V$ where the UPD is assumed to be nil, to the final E_f in the UPD range (Fig. 21) always with E_f less negative than $E_{eq(Pb/Pb^{2+})}$. We describe potentiostatic transient of lead UPD on polycrystalline silver without chloride added to the solution. We have planned to study the effect of chloride ions on the transient experiments in the future. The understanding of the thermodynamic and kinetic effects of chloride on lead UPD and its correlation with the inhibition of $CrCl_3$ reduction on silver will point towards an understanding of the role of chloride in the latter process. A rotating silver disk electrode (RDE) has been used in order to define the mass transport conditions since the solution for the convective-diffusion differential equation is known in this case. In this way, current transients were recorded as shown in Figs. 22 and 24.

Fig. 22 shows the inhibiting effect of lead concentration on $CrCl_3$ electroreduction at constant potential and rotation frequency. The discrepancy at t=0 in the observed cathodic current for $CrCl_3$ reduction (the contribution of lead UPD current is neglected) with and without lead in solution is not very well understood. It is possible, though, that at -0.1V, where the electrode is held, significant lead is present on the surface, or that some irreversible lead deposition occurs, producing a surface alloy and causing this irreproducibility. Another possibility is a difference in hydrogen evolution with and without lead present. However, from the study of $CrCl_3$ on pure silver, a hydrogen current at -0.7V as large as 100 μA (Fig. 7) is not expected. The increase of lead concentration in solution reduces the time scale for the inhibition effect on Fig. 22.

Fig. 23 shows similar transients at constant lead concentration in solution and constant rotation frequency. The effect of electrode potential is evident; the more cathodic the electrode potential, the higher the $CrCl_3$ reduction current. The effect of simultaneous UPD lead is similar at all potentials; note the same time constant for this effect. The electrode potential affects more the redox couple than the UPD effect. This is probably due to lead UPD being under convective-diffusion conditions whereas the redox couple shows diffusion-kinetic control. However, one should expect an increase in lead coverage with cathodic potential in the steady state.

Fig. 24 shows the effect of rotation frequency on the potentiostatic transient at constant lead concentration and potential. An inversion in the order of curves is obtained in a narrow time range. Before this, an increase in current with rotation is observed, as expected from the partial diffusion control of the reduction current for the redox couple. After the inversion, the cathodic current dies away more rapidly the faster the electrode is rotated. The crossing-over effect can be explained by assuming that $CrCl_3$ reduction and UPD are both affected by convective diffusion. At short times, due to the low lead coverage, low inhibition is observed and the chromium reduction currents are close to the Levich limiting current values and therefore strongly rotation-dependent. As lead coverage increases with time, the Cr(III) reduction current decreases into the predominantly kinetic regime and is strongly inhibited by UPD lead. The build-up of the UPD layer only reduces convective-diffusion control. Based on this model of the system, a quantitative treatment is developed.

At constant potential (potential step method), the cathodic current for $CrCl_3$ reduction in the presence of simultaneous Pb UPD can be described by:

$$i = \int_{t=0}^{t} \left(\frac{di}{d\theta}\right)_E \left(\frac{d\theta}{dt}\right) dt \qquad (8)$$

where θ refers to the UPD lead coverage. The term $(d\theta/dt)$ is readily evaluated only if under pure diffusion control. Since the convective-diffusional flux j_{Pb} is known,

$$n_T \frac{d\theta}{dt} = -j_{Pb} = -D\left(\frac{\partial C_{Pb}}{\partial x}\right)_{x=0} = -D\left[\frac{C_b - C_s}{\delta}\right] \qquad (9)$$

with

$$\delta = 1.61\ D_{Pb^{2+}}^{-1/3}\ \nu^{1/6}\ \omega^{-1/2}$$

for the RDE. For pure diffusion control, $C_s = 0$, the surface concentration of lead is zero.

It is desirable to avoid any kinetic control of formation of UPD layer during the potential-step experiment since this requires more data and complicates the analysis. The complex voltammetry curve for UPD lead formation indicates such.

The simplest model for the effect of Pb(UPD) on Cr(III) reduction is the surface blockage by the foreign adsorbate (lead) (11,12).

$$k = k_o(1-\theta_{Pb}) + k_u\theta_{Pb} \qquad (10)$$

and the rate constant on the lead ad-atoms will be assumed small, i.e.,

$$k_u\theta_{Pb} \ll k_o(1-\theta_{Pb})$$

Otherwise one must introduce adjustable parameters arising from the quite complex isotherm needed to describe lead UPD. A knowledge of the UPD lead transient in the absence of the redox couple is required, $\theta_{Pb} = f(t)$, to interpret the inhibiting effect on the reduction current i_{Cr} as a function of time.

The observed cathodic currents for $CrCl_3$ reduction can be corrected for mass transport by means of the equation

$$\frac{1}{i_{obs}} = \frac{1}{i_k} + \frac{1}{B\,C_b}\,\omega^{-1/2} \tag{11}$$

where i_{obs} is the measured current for $CrCl_3$ reduction, i_k the electro-kinetic current, $B=0.62nFAD^{2/3}\nu^{-1/6}$ and C_b the bulk concentration. The use of the Koutechy-Levich equation is justified experimentally as can be seen in the insert in Figure 24.

C. Lead UPD on Silver

Fig. 25 shows current transients with the potential stepped from -0.10V (UPD is assumed to be negligible) to different potentials in the UPD region (a-e) and also to potentials more cathodic than the Nernst potential -0.525 V(SCE) (f) with RDE (ω=900 rpm). After double-layer charging, the current transients can be interpreted in terms of convective diffusion first, and then mixed diffusion-kinetics.

Fig. 26 depicts the charge obtained by integrating the current transients as a function of time. Initially, convective diffusion prevails, as seen from the initial linear region of the q-t curves, whose gradients yield a diffusion constant for Pb^{2+}, D = 9.6 x $10^{-6}cm^2s^{-1}$, using the equation

$$q_{linear} = (0.62\,\gamma\,FAD^{2/3}\,\nu^{-1/6}\,C_b\,\omega^{1/2})t \tag{12}$$

with γ the electrosorption valence of Pb UPD and all other symbols with their usual meaning. This is in good agreement with data reported by Vicent and Bruckenstain (14):

$$D_{Pb^{+2}} = 9.7 \times 10^{-6}\ cm^2s^{-1}$$

in 0.5M KCl, 10^{-4}M HCl.

The transient charge curves depart from the behavior expected for pure convective-diffusion control at longer times and level off towards their equilibrium value q_{eq}, which increases with cathodic potential. Bruckenstain has suggested for Ag UPD on gold that convective-diffusion conditions are valid before monolayer coverage is reached (13). The electrosorption valence is not known and hence the charge is not necessarily a measure of Pb(UPD) surface concentration. At high coverage, however, the electrosorption valence does approach closely -2, and hence the charge is indicative of surface concentration. Thus,

$$q = - \gamma F \Gamma$$

where Γ is the surface excess, and the coverage

$$\theta = \frac{\Gamma}{\Gamma_{monolayer}} = \frac{q}{q_{monolayer}}$$

at γ = constant. The curves in Fig. 25 give evidence of some complications that may reflect low level impurities such as oxygen. The data plotted in Fig. 26 has been corrected for background currents.

From the charge of Pb UPD monolayer calculated for a close-packed model on silver 300 μ coul cm^{-2} (15) and the equilibrium values in Fig. 26, one concludes that more than a monolayer is formed (the roughness factor has not been measured in the present experiments). This seems to be reasonable in view of the near total supression of the $CrCl_3$ reduction at long times (Figs. 22-24) for a strong inhibition on Pb(UPD) site (i.e., Equation 10). Future experiments with RRDE and chloride ion in solution will determine the value of γ and its dependence on potential and chloride ion concentration.

In the potentiostatic transient experiments at a given potential, γ is assumed to be constant and q proportional to θ. It is possible that changes in γ can contribute to the charge transient; however, this effect is probably secondary.

In Fig. 26, after correction for background current, there is still an intercept of some 6μ coul which is not expected from the UPD experiment. One calculates the initial charge corresponding to Pb^{2+} in the diffusion layer volume at $\omega = 900$ rpm when the potential is changed into the UPD region to be

$$V = Z_D \cdot A = 7.05 \times 10^{-4} \text{ cm}^3$$

$$Z_D = 1.61 \, \omega^{-1/2} \, \nu^{1/6} \, D^{1/3} = 3.53 \times 10^{-3} \text{ cm}$$

and $m = VC$, with $D = 6.9 \times 10^{-6} \text{ cm}^2\text{s}^{-1}$, and

$$q_{initial} = \gamma \, Fm \sim 1\mu \text{ coul}$$

for $\gamma = z$. This value is less than the 6μ coul found, and we believe this is due to double-layer charging effects. This aspect will be considered in the future.

Fig. 27 shows the effect of rotation rate on lead UPD transients at constant potential and lead concentration in solution. The concentration of Pb^{2+} is higher and hence kinetic control is much more important. There is an inversion point before which current increases with rotation and after which the current decreases with increasing rotation rate.

The transient behavior is rather similar althouth there are quantitative differences due to the higher Pb^{2+} concentration and the more important role of the kinetics of the UPD process in Figs. 25 and 27. The corresponding charge transients obtained by geometric integration of the i-t curves are shown in Fig. 28 with the background current subtracted.

It is evident that the rate of charge increase with time depends on rotation, but the low sensitivity of the integrated curves to the inflexion point precludes it being shown in Fig. 28.

Analysis of Figs. 27 and 28 shows that, at the beginning of the transient, an increase of charge is observed with increased rate of convective-diffusion. However, the opposite is observed at longer times

when some kinetic step becomes rate-determining. Since at t→∞ the equilibrium charge should be constant at constant potential,

$$q_{eq}(E) = \int_0^\infty i(t)\, dt = \text{constant} \qquad (13)$$

the excess charge at h₁ ₁ rotation before the inversion point in Fig. 27 should be balanced by an equal charge after that point if a sufficiently long-time experiment is performed. Furthermore, Fig. 28 should show a convergence towards a constant q_{eq} value independent of the rotation frequency and only dependent on the applied potential and the ·ead concentration in solution.

Inspection of Figs. 27 and 28 shows that this condition is probably fulfilled at sufficiently long times.

The crossing-over point can be interpreted on the basis of kinetic control becoming important. In the time scale before this becomes important, the deposition of lead under convective-diffusion conditions yields a non-equilibrium (between surface and solution) coverage since, for a given potential $q=f(\omega)$. The electrosorption valence is a function of surface concentration in the short time scale. A surface rearrangement of the UPD layer occurs at various coverages and can be relatively slow, thus affecting the kinetics of adsorption. At sufficiently long times, rearrangement of the equilibrium coverage is finally reached, corresponding to E and C_{Pb}^b.

In order to get a mathematical description of the i-t transients for UPD lead on silver, and subsequently to use it to model the inhibiting effect on $CrCl_3$ reduction, two models will be considered.

Model I

We consider the surface process:

$$Pb^{2+} + (2-y)e^- \underset{k_{-1}}{\overset{k_1}{\rightleftharpoons}} Pb^{y+}_{ads} \qquad (14)$$

coupled to convective diffusion.

The rate of coverage change is given by (Langmuirian kinetics):

$$\frac{d\theta}{dt} = k_1 C_s (1-\theta) - k_{-1}\theta = B\,\omega^{1/2}(C_b - C_s) \tag{15}$$

with $B = 0.62 D^{2/3} \nu^{-1/6}$ where C_b and C_s are the bulk and surface concentrations of Pb^{2+}, respectively.

We simplify Equation (15) for low coverage $\theta \ll 1$, and the solution of the differential equation with the following boundary conditions:

At $t=0$: $\theta=0$; $q=0$ $C_s = C_b$

At $t=\infty$: $\theta=\theta_\infty$; $q=q_\infty = FA\Gamma_\infty \gamma$; $C_s = C_b$

is

$$-\ln[1 - q/q_\infty] = \left(\frac{B\,k_{-1}\,\omega^{1/2}}{k_1 + B\omega^{1/2}}\right)t \tag{16}$$

The electrosorption valence γ is assumed to be a constant at constant potential.

The slope of Equation (16) should fulfill:

$$\frac{1}{S} = \frac{1}{k_{-1}} + \frac{k_1}{k_{-1}B}\,\omega^{-1/2} \tag{17}$$

Hence, from a plot $1/S$ vs $1/\omega^{1/2}$, k_1 and k_{-1} can be evaluated. For k_1, $k_{-1} \gg B\omega^{1/2}$, the convective-diffusion limit is obtained:

$$-\ln[1-q/q_\infty] = B\,\omega^{1/2}t$$

Model II

Reaction 14 is assumed to be in fast equilibrium and the rate-determining process is a subsequent step (irreversible surface reaction):

$$Pb_{ads}^{y+} + (y-y')e^- \xrightarrow{k_s} Pb_{ads}^{y'+} \tag{18}$$
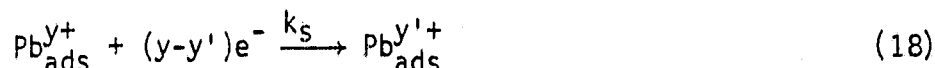
This assumes the existence of two adsorption sites, and using Langmuir-type kinetics:

$$\frac{d\theta}{dt} = k_s(1-\theta')\frac{k_1}{k_{-1}} C_s = B \omega^{1/2}(C_b-C_s) \tag{19}$$

The solution of Equation (19) with the same boundary conditions as for Case 1, making $k_1/k_{-1}=K$, and assuming $\theta \ll 1$ in the calculation of C_s is:

$$-\ln[1 - \frac{q}{q_\infty}] = (\frac{k_s K B \omega^{1/2}}{k_s K + B \omega^{1/2}}) C_b \cdot t \tag{20}$$

and in analogy with model I, the slope of $-\ln[1 - \frac{q}{q_\infty}]$ vs t plot follows

$$\frac{1}{S} = \frac{1}{k_s K C_b} + \frac{1}{B C_b} \omega^{-1/2} \tag{21}$$

For $K k_s \gg B \omega^{1/2}$, the convective-diffusion limit is obtained:

$$-\ln[1 - \frac{q}{q_\infty}] = (B \omega^{1/2} C_b) \cdot t \tag{22}$$

From the similar shape of Equations (16) and (17) and Equations (20) and (21), it can be concluded that for the analysis of the potentiostatic UPD transient plots of $-\ln[1-q/q_\infty]$ vs t and $1/S$ vs $\omega^{-1/2}$ should yield straight lines from which kinetic and diffusion parameters can be obtained.

Fig. 29 shows a $-\ln[1-q/q_\infty]$ vs t plot corresponding to the transient data of Fig. 25 for low lead concentration. It can be seen that pure convective-diffusion conditions common to both potentials are observed initially (slope given by Equation (16)), but then kinetic-diffusion coupling is evident.

More interesting is the result for more concentrated solutions where pure diffusional conditions are not observed and $-\ln[1-q/q_\infty]$ vs t plots yield straight lines at different rotation frequencies (Figs. 30 and 31) in good accord with Equations (16) and (20) for each of the models. The dependence on rotation rate of the inverse slopes $1/S$ vs $\omega^{-1/2}$ shown in Fig. 32 is a linear one, slope S' and the intercepts are dependent on potential; however, the dependence on potential is very small for S'.

In terms of Models I and II, the $1/S$ vs $\omega^{-1/2}$ plots have some diagnostic value

Table 1

	Model I	Model II
J'	$1/k_{-1}$	$1/(k_s\ K\ C_b)$
S'	$k_1/(k_{-1}B)$	$1/(B\ C_b)$

Model II is favored in terms of the high i_o values reported for UPD phenomena (Reaction 14) and the time scale of the potentiostatic transients. However, the potential dependence on S' expected from Model I is given by:

$$\frac{k_1}{k_{-1}} = k^o\ \exp\left(\frac{F}{RT}\ E\right)$$

For a small potential change (Fig. 32), one expects

$$\frac{S_1'}{S_2'} = \exp\left[\frac{F}{RT}\ (E_1 - E_2)\right]$$

The value obtained from Fig. 32 is 1.12 and therefore no unambiguous distinction of both models can be made. For Model I, one calculates:

	E (SCE)	
	-0.45V	-0.50V
$k_1(cm/s^{-1})$	1.09×10^{-2}	1.17×10^{-2}
$k_{-1}(s^{-1})$	0.53	0.50

The mathematical treatments according to Models I and II are based on Langmuirian-type adsorption-desorption kinetics. This treatment can only be viewed as a first stage in the theoretical approach to the problem. While linearity is observed in the plots depicted in Figs. 30 and 31,

this may well be a particularly low sensitivity test of the validity of the kinetic model. The complex nature of the UPD voltammetry curves is evidence of the complexity of the adsorption-desorption isotherm and the associated kinetics.

D. Analysis of Simultaneous Lead UPD Inhibition on $CrCl_3$ Reduction

Comparison of potentiostatic transients for $CrCl_3$ reduction with simultaneous lead UPD with transients due to lead UPD in the absence of $CrCl_3$ in solution (Figs. 22-24 with 25 and Fig. 34 with 27) under similar conditions shows that the inhibition effect occurs in the time scale of lead UPD. Furthermore, from comparison of Figs. 34 and 28, one concludes that the rate of the $CrCl_3$ reduction is supressed to a very small value at high lead coverages.

In Fig. 34, the observed currents are always below the convective-diffusion level, and since kinetic-diffusion coupling is observed for $CrCl_3$ flux, correction for mass transport is obtained with Equation (11), (i_k).

From Equation (10a), with the assumption that $k_u \theta_{Pb} << k_o (1-\theta_{Pb})$, one expects that the kinetics of chromic ion reduction current decreases as $(1-\theta_{Pb})$ decreases at constant potential. However,

$$1 - \theta_{Pb} = 1 - q/q_\infty \tag{23}$$

assuming $q_\infty = q_{monolayer}$. From Equations (16) and (20),

$$-\ln(1-\theta_{Pb}) = St \tag{24}$$

with

$$S = \frac{B \, k_{-1} \omega^{1/2}}{k_1 + B \, \omega^{1/2}} \qquad \text{for Model I}$$

$$S = \frac{k_s \, K \, B \, \omega^{1/2}}{k_s K + B \, \omega^{1/2}} \, C_b \qquad \text{for Model II}$$

Therefore, from Equations (10), (16), (23) and (24):

$$\ln i_k = \ln i_k^0 - St \tag{25}$$

with i_k^0 the kinetic $CrCl_3$ reduction current in the absence of simultaneous UPD. The S term will account for the simultaneous kinetic-diffusion lead UPD.

Figs. 33 and 35 show $\ln(i_k)$ vs. t plots for $CrCl_3$ reduction data shown in Figs. 24 and 34, respectively. Good linearity, common intercept (i_k^0) and dependence on rotation frequency are found, as predicted by Equation (25). Furthermore, the inverse of the slopes S in Figs. 33 and 35 should follow the equation:

$$\frac{1}{S} = J' + S' \omega^{1/2} \tag{26}$$

with values indicated in Table II.

<u>Table II</u>

	Model I	Model II
J'	$1/k_{-1}$	$1/(k_s K C_b)$
S'	$k_1/(k_{-1}B)$	$1/(B C_b)$

•(slope and intercept based on Figs. 36 and 37)

Note that the data in Table II obtained from the analysis of the $CrCl_3$ reduction current transients where the lead current is negligible should have been the same as that obtained from lead UPD transients. This is due to the fact that the $CrCl_3$ reduction current is directly a measure of the lead coverage. However, comparison of Figs. 32 and 37 shows that this is not the case; S' and J' are smaller for $CrCl_3$ than for lead UPD. This is expected since the UPD data has been obtained without chloride ion in solution. If chloride and lead ions show competitive adsorption, the chloride will affect the UPD kinetics and hence the lead coverage transient resulting in a different inhibition transient, even though the pattern seems not to be altered qualitatively.

Chloride ion seems to moderate the effects seen in Fig. 27 (crossing over with rotation speed). In any case, these are secondary effects and the inhibition model appears to be a reasonable first approximation.

Future experiments are planned with chloride in order to test this point. The study of the combined effect of chloride and lead UPD on chromium redox couple is expected to unravel the role of chloride ions.

V. DISCUSSION

Chloride in the inner coordination sphere of chromium(III) aquocomplexes is needed for the reduction to occur before significant hydrogen evolution is observed on gold and silver electrodes. Free chloride does not seem to play a role in enhancing the reaction rate for the $Cr(OH_2)_6$ or $CrCl(OH_2)_5^{2+}$. On gold electrode the presence of a maximum in the steady state current-potential curve can be explained by a halide bridging mechanism and conformational effects dependent on the electrode potential. Lead UPD simultaneous to the reduction of $CrCl_3$ reduction has an inhibiting effect on the kinetics of this couple. Fairly good correlation has been presented for a model where the reduction of $CrCl_3$ takes place on the lead free sites and is almost totally inhibited on lead sites, thus suggesting a reaction-site effect.

To a first approximation it is accepted that UPD layers affect strongly catalytic reactions by changing the properties of surface reaction intermediates such as in the case of O_2 reduction and formic acid oxidation (17). On the other hand, the electron transfer process in outer sphere reactions is not affected by UPD ad-atoms, other than through change in double layer properties.

In perchlorate solutions and in the absence of chloride ions in solution, the work function of Ag decreases with lead UPD coverage (18) and capacitance

measurements showed that for coverages close to the monolayer the double layer properties are similar to those of polycrystalline lead (19). A strong and complex interaction of lead UPD with adsorbed chloride associated to a collective phenomenon has been reported by Gerischer and Kolb (16).

The inhibiting effect of lead UPD on $CrCl_3$ reduction can probably be explained by a stronger interaction of the chloride in the inner coordination sphere of Cr^{+3} with the silver than with the lead. The UPD lead can lead to an increase in the barrier height for the Cl^- bridging electron transfer reaction and thus an inhibiting effect. Further, the weaker interaction with Pb UPD will result in a decreased surface concentration of the Cr-Cl complexes.

VI. APPENDIX I

Evaluation of relative concentrations of chromium complexes in aqueous solutions. For the reactions:

$$CrCl_2(H_2O)_4^{2+} \underset{k_{-1}}{\overset{k_1}{\rightleftharpoons}} CrCl(H_2O)_5^{+} \overset{k_2}{\longrightarrow} Cr(H_2O)_6^{3+}$$
$$+ Cl^{-} \qquad\qquad + Cl^{-}$$
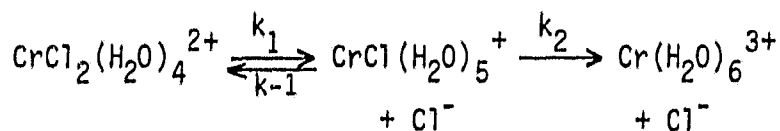
the kinetic equations are:

$$\frac{dc_1}{dt} = -k_1 c_1$$

$$\frac{dc_2}{dt} = k_1 c_1 - k_2 c_2$$

and

$$\frac{dc_3}{dt} = k_2 c_2$$

with c_1, c_2 and c_3, respectively, the concentrations of $Cr(H_2O)_4Cl^{2+}$, $Cr(H_2O)_5Cl^{+}$ and $Cr(H_2O)_6^{3+}$ and c_T the total chromium concentration in solution.

We have neglected the backreactions (k_{-1} and k_{-2}) in this treatment.

Solving the differential equations with the corresponding initial and boundary conditions:

$$t = 0 \quad c_1 = c_T \quad c_2 = 0 \quad c_3 = 0$$
$$t = \infty \quad c_1 = 0 \quad c_2 = 0 \quad c_3 = c_T$$

the respective molar fractions c_i/c_T are:

$$\frac{c_1}{c_T} = \exp(-k_1 t)$$

$$\frac{c_2}{c_T} = \frac{k_1}{k_2 - k_1} \left[\exp(-k_2 t) - \exp(-k_1 t) \right]$$

the maximum will occur for $\dfrac{dc_2}{dt} = 0$

and hence

$$t_{max} = -\frac{\ln k_2/k_1}{k_2 - k_1}$$

$$\frac{c_3}{c_T} = 1 + \frac{k_2}{k_1 - k_2}\exp(-k_1 t) - \frac{k_1}{k_1 - k_2}\exp(-k_2 t)$$

VII. REFERENCES

1. J. Weber, Z. Samec, V. Marecek, J. Electroanal. Chem. 89 (1978) 271.

2. P.J. Elving and B. Zemel, J. Am. Chem. Soc.

3. J. Lewis and R.G. Wilkins, "Modern Coordination Chemistry", 146 (1960), Interscience Publishers, Inc., New York.

4. P.J. Elving and B. Zemel, J. Am. Chem. Soc, 79 (1957) 1281.

5. D.A. Johnson and M.A. Reid, Electrochemical Society Fall Meeting, Extended Abstracts A252, 405 (1982).

6. V.G. Levich, "Physicochemical Hydrodynamics", Prentice Hall (1962).

7. A. Hamelin, T. Vitanov and A. Popov, J. Electroanal. Chem., 145 (1983) 225.

8. S. Donovan and E. Yeager, "The Electrode Kinetics of Chromous-Chromic Couple", O.N.R. Technical Report No. 24, October, 1969.

9. W.J. Albery and M.L. Hitchman, "Ring-Disc Electrodes", Oxford University Press (1971).

10. W.J. Albery and S. Bruckenstein, Trans. Faraday Soc., 62, 1920 (1965).

11. R.W. Schmid and C.N. Reilley, J. Am. Chem. Soc. 80, 2087 (1958).

12. J. Weber, J. Koutecky and J. Koryta, Z. Elektrochem. 63, 583 (1959).

13. T.M. Riedhammer, L.S. Melricki and S. Bruckenstein, Z. Phys. Chemie, NF. III, 177 (1978).

14. V.A. Vincente and S. Bruckenstein, Anal. Chem., 45 (1973) 2036.

15. K. Takayanagi, D.M. Kolb, K. Kambe and G. Lehmpfuhl, Surface Science, 100 (1980) 407.

16. D.M. Kolb, M. Przasnyski and H. Gerischer, Soviet Electrochem., 13 (5) 600 (1977).

17. "Electrocatalytic Effects of Foreign Metal Ad-Atoms", R.R. Adzic, Bull. Soc. Chim., Beograd, 48 (3) 1 (1983).

18. K. Takayanagi, D.M. Kolb, K. Kambe and G. Lehmpfuhl, Surface Science, 100 (1980) 407.

19. J.T. Hupp, D. Larkin, H.Y. Liu, and M.J. Weaver, J. Electroanal. Chem., 131 (1982) 299.
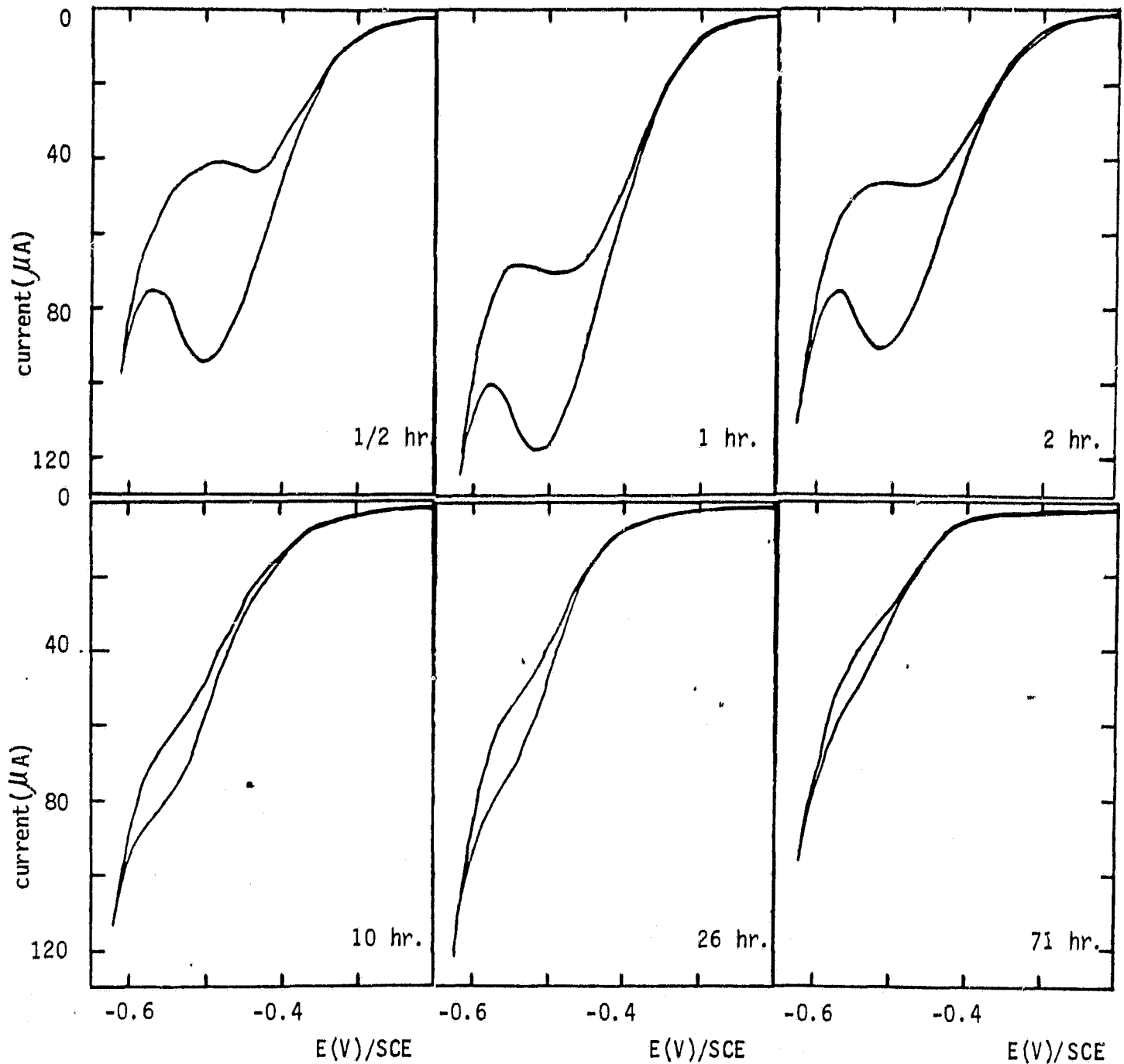
Figure 1: Cyclic voltammetry of 4.8 mM $CrCl_3$ in 0.01 M $HClO_4$ and 0.1 M $NaClO_4$ deareated solution on gold rotating disk electrode(A=0.196 cm^2; rotation rate: 900rpm). Experiments were carried out at the different times indicated after $CrCl_3$ was disolved and added to the solution.
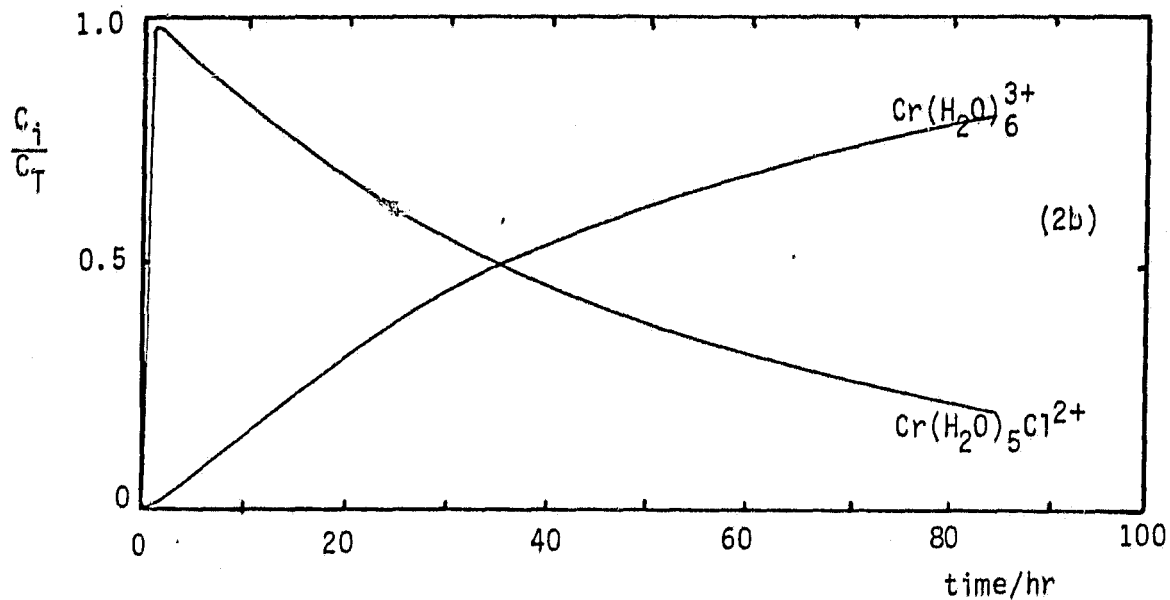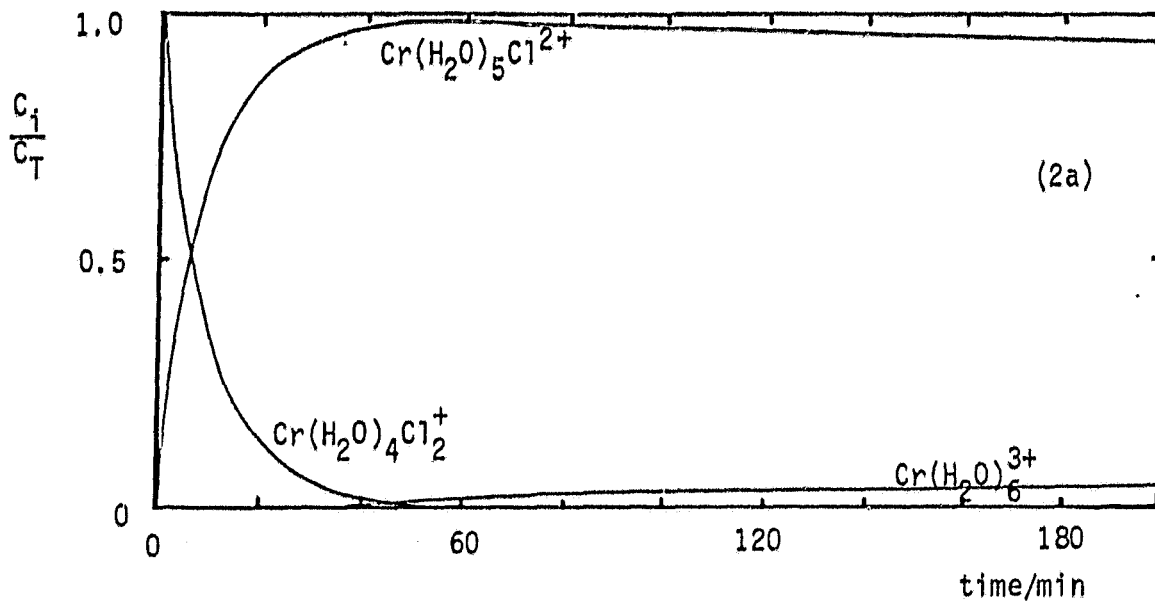
Figure 2: Molar fraction C_i/C_T of the different constituents of $CrCl_3$ solution as a function of time after dissolution in water; calculated in Appendix I. (Fig. a is an enlarged section of Fig. b)
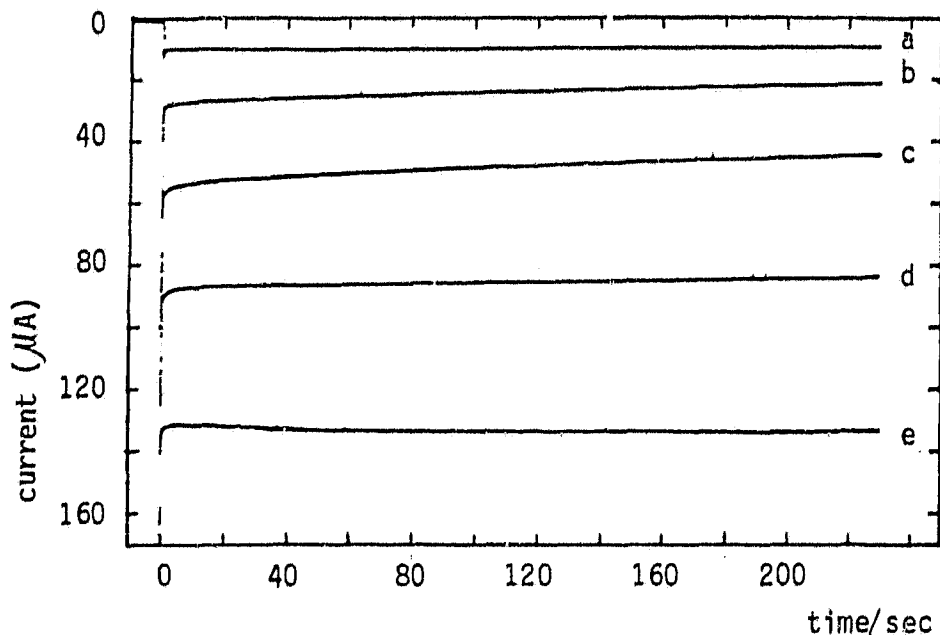
Figure 3: Potentiostatic transients of 4.8 mM $CrCl_3$ in 0.1 M $NaClO_4$ and 0.01 M $HClO_4$ deaireated solution on gold rotating disk electrode (A=0.196 cm^2; rotation rate: 900 rpm). From 0.0 V to a) -0.30V ; b) -0.35V ; c) -0.40V; d) -0.45V and e) -0.50V.
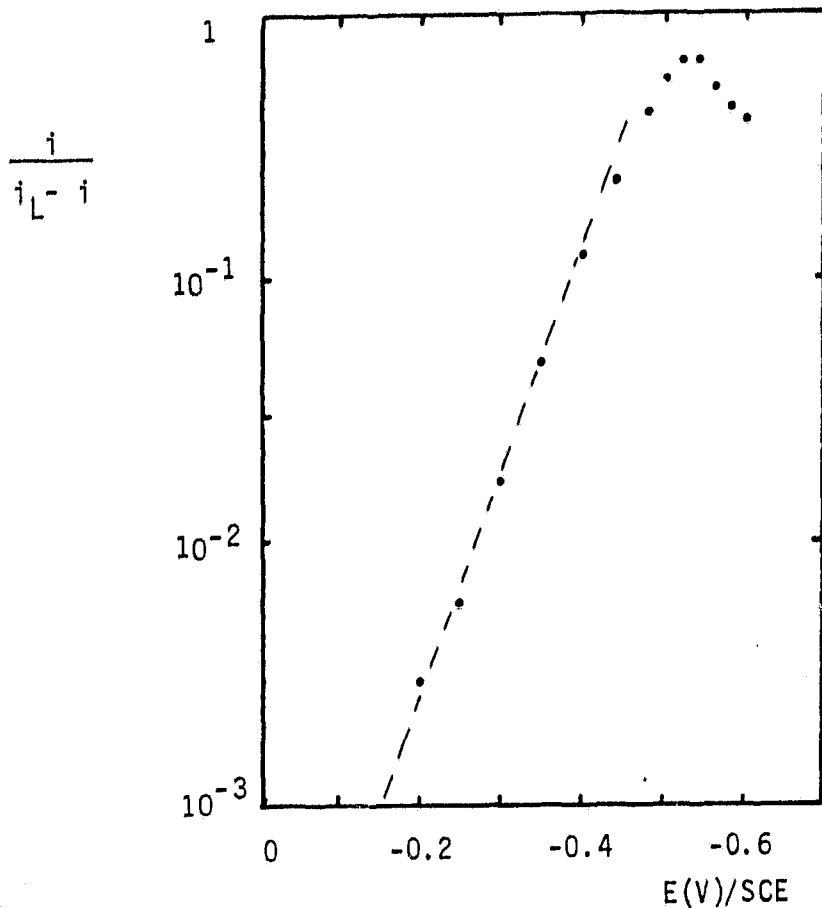
Figure 4: Steady state Tafel plot for 4.8 mM $CrCl_3$ reduction
on gold rotating disk electrode (A=0.196 cm^2;
rotation rate: 900 rpm; i_L=0.63 mA) in 0.1 M $NaClO_4$
and 0.01 M $HClO_4$.
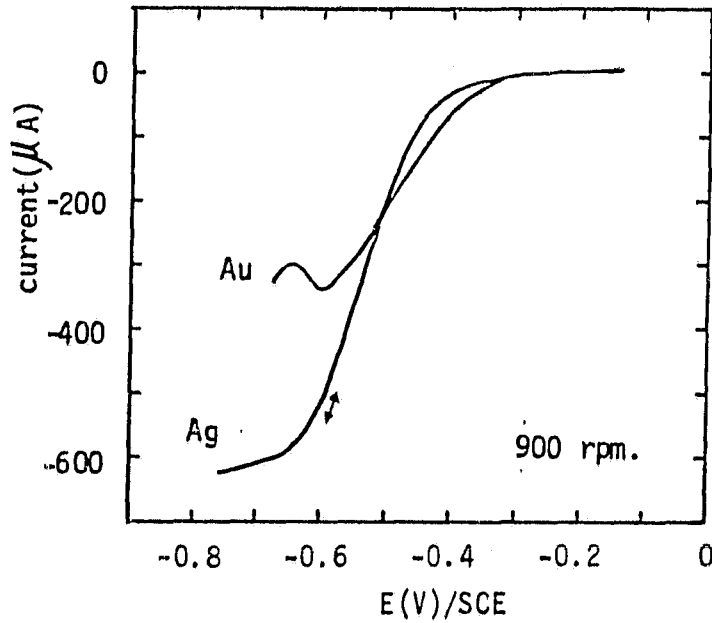
Figure 5: Polarization curves for $CrCl_3$ reduction on gold
and silver disk electrode. Solution: 0.1 M $NaClO_4$,
0.01 M $HClO_4$ and 7mM $CrCl_3$. Electrode areas:
0.196 cm^2. Sweep rate: 10 mV/s. The reverse scan
on gold has been omitted.
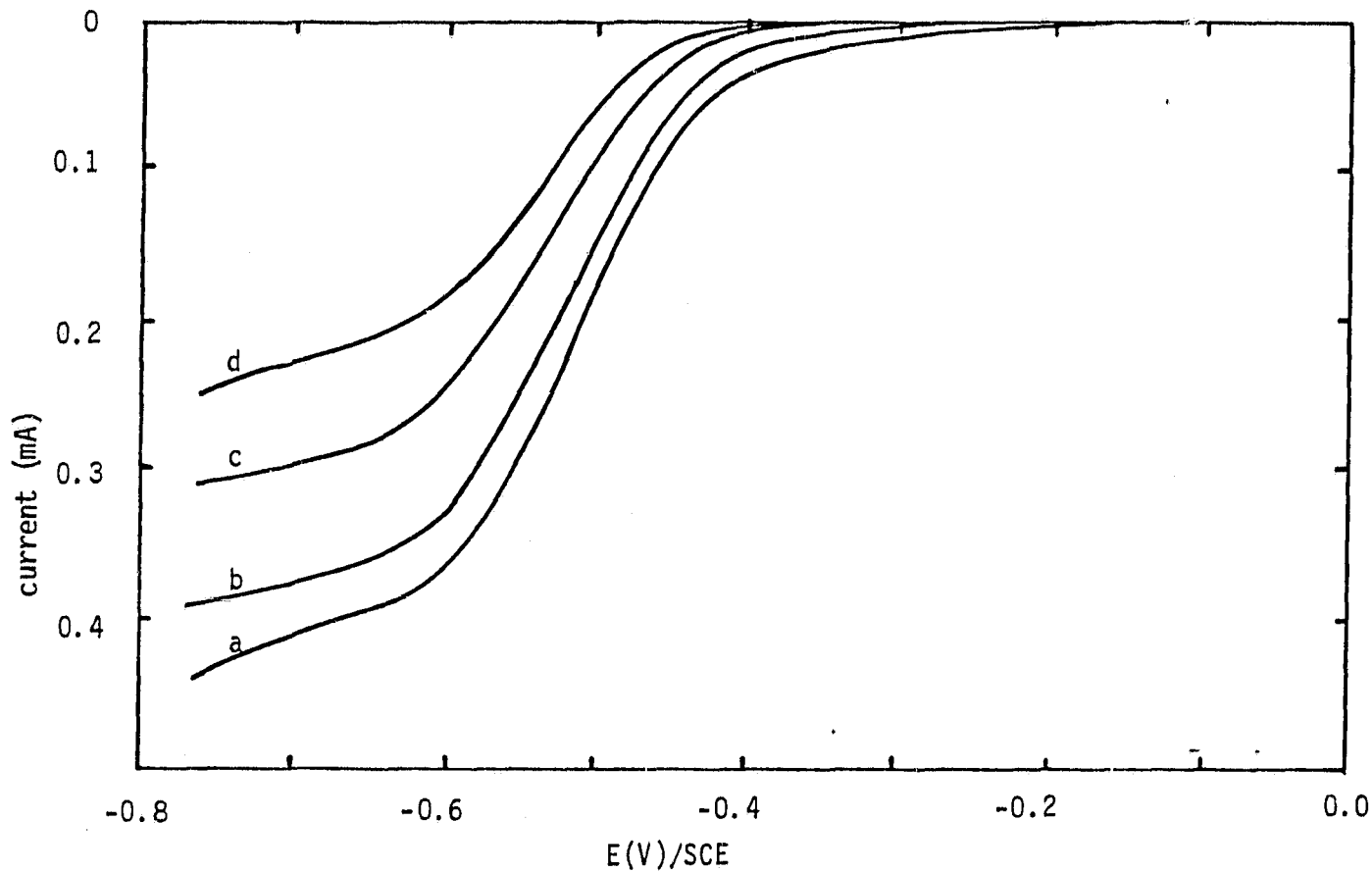
Figure 6: Polarization curves for the reduction of $CrCl_3$ in 0.1 M $NaClO_4$ and 0.01 M $HClO_4$ deaireated solution on silver rotating disk electrode (A=0.196 cm^2; rotation rate: 900 rpm) at different times after $CrCl_3$ was disolved. a) 0.5 and 2 hours
　　　　　　　　　　　　　　b) 3 hours
　　　　　　　　　　　　　　c) 15 hours
　　　　　　　　　　　　　　d) 42 hours
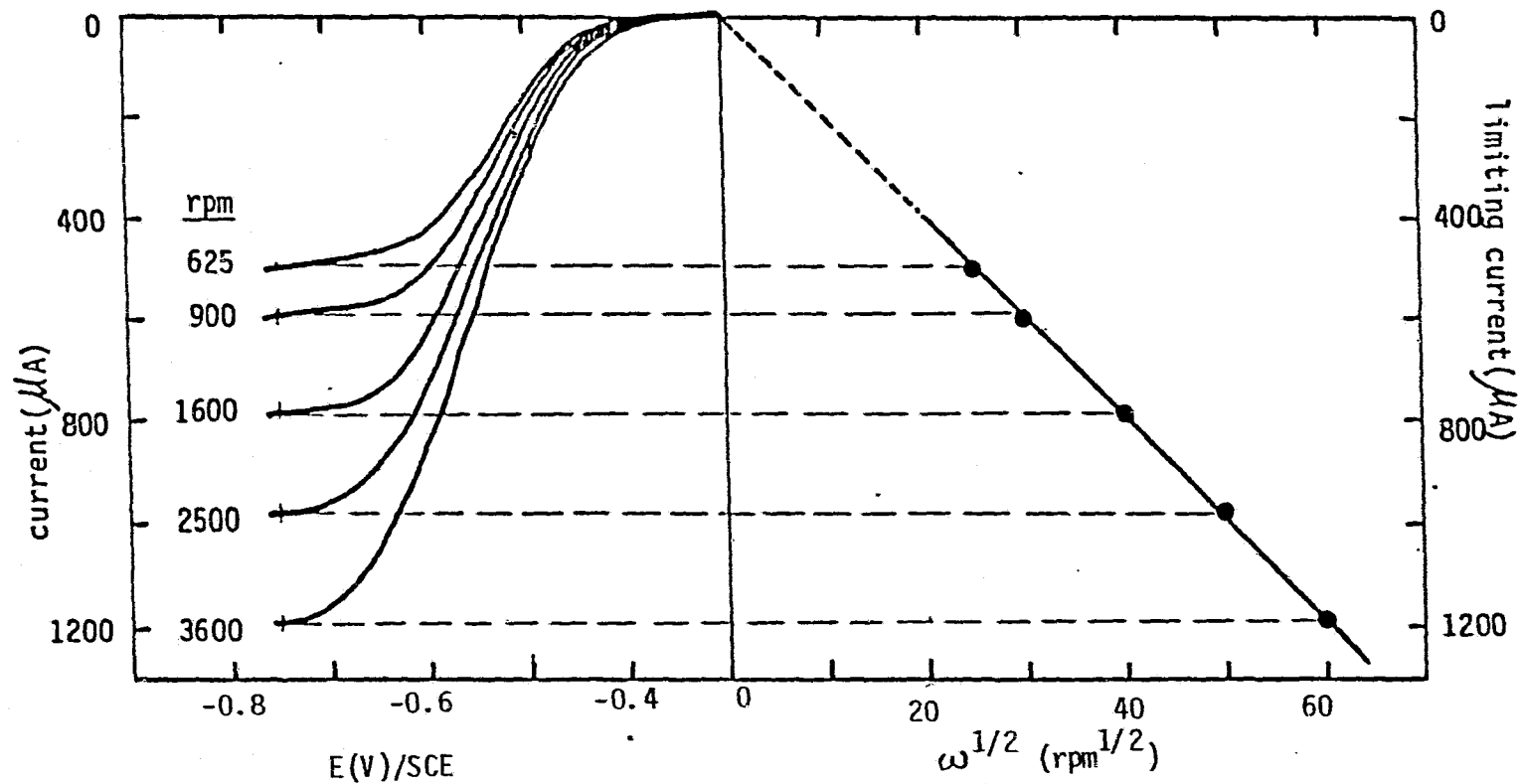
Figure 7: Polarization curves and corresponding i_L vs. $\omega^{1/2}$ plot for 7 mM $CrCl_3$ reduction on silver disk electrode. Electrolyte: 0.1 M $NaClO_4$ and $HClO_4$ (pH= 2.2). Sweep rate: 10 mV/s. Electrode area: 0.196 cm^2.
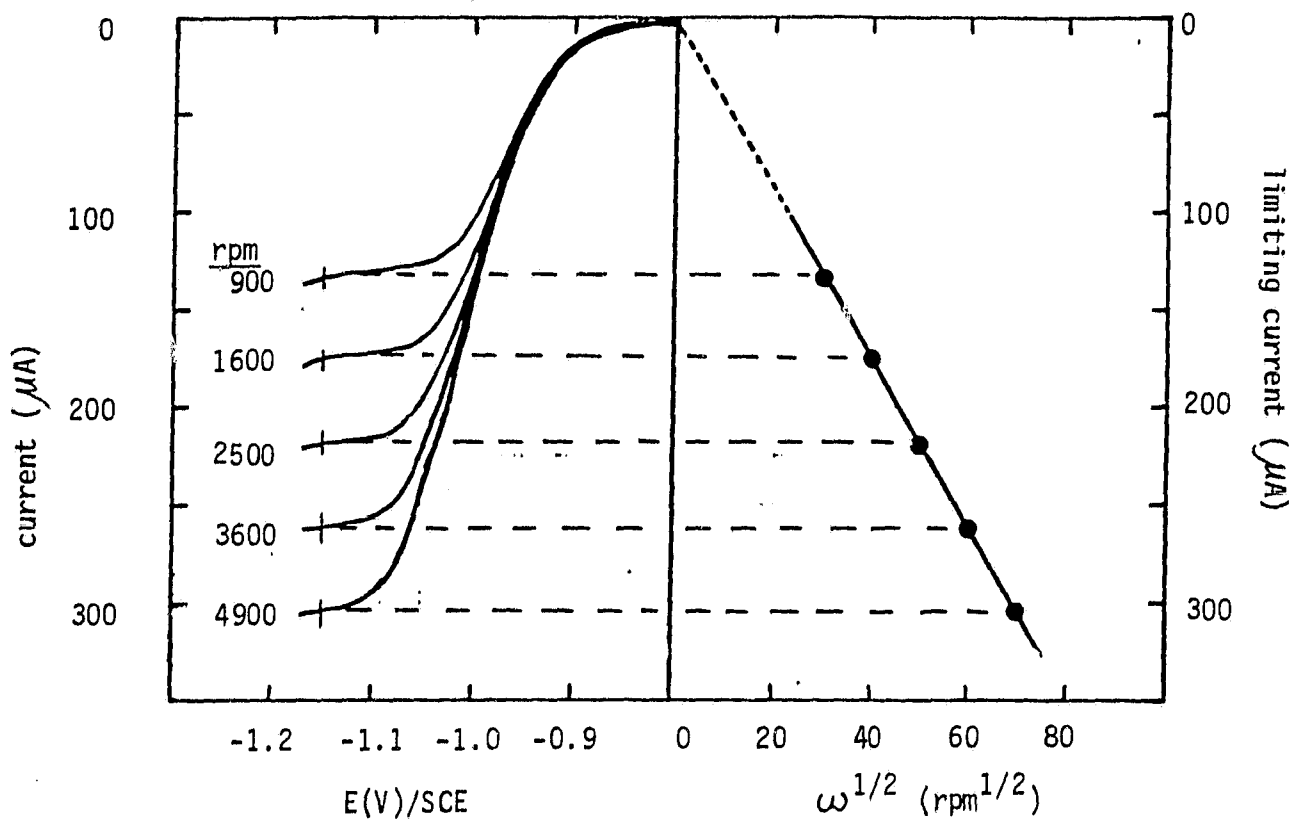
Figure 8: Polarization curves and corresponding i_L vs. $\omega^{1/2}$ plot for
0.61 mM $Cr(ClO_4)_3$ reduction on Ni(Hg) rotating disk electrode
(A= 0.28 cm^2). Electrolyte: 2 mM $NaClO_4$ and 9 mM $HClO_4$.
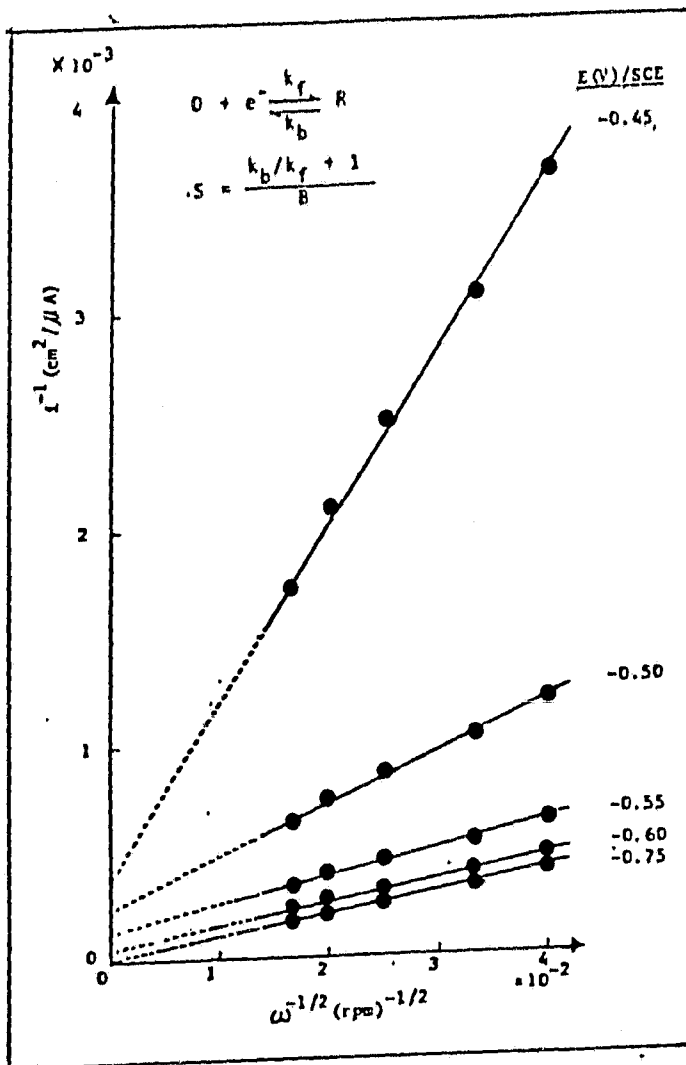
Figure 9: 1/i vs. $1/\omega^{1/2}$ plots for $CrCl_3$ reduction on silver electrode. Data taken from Fig. 7.
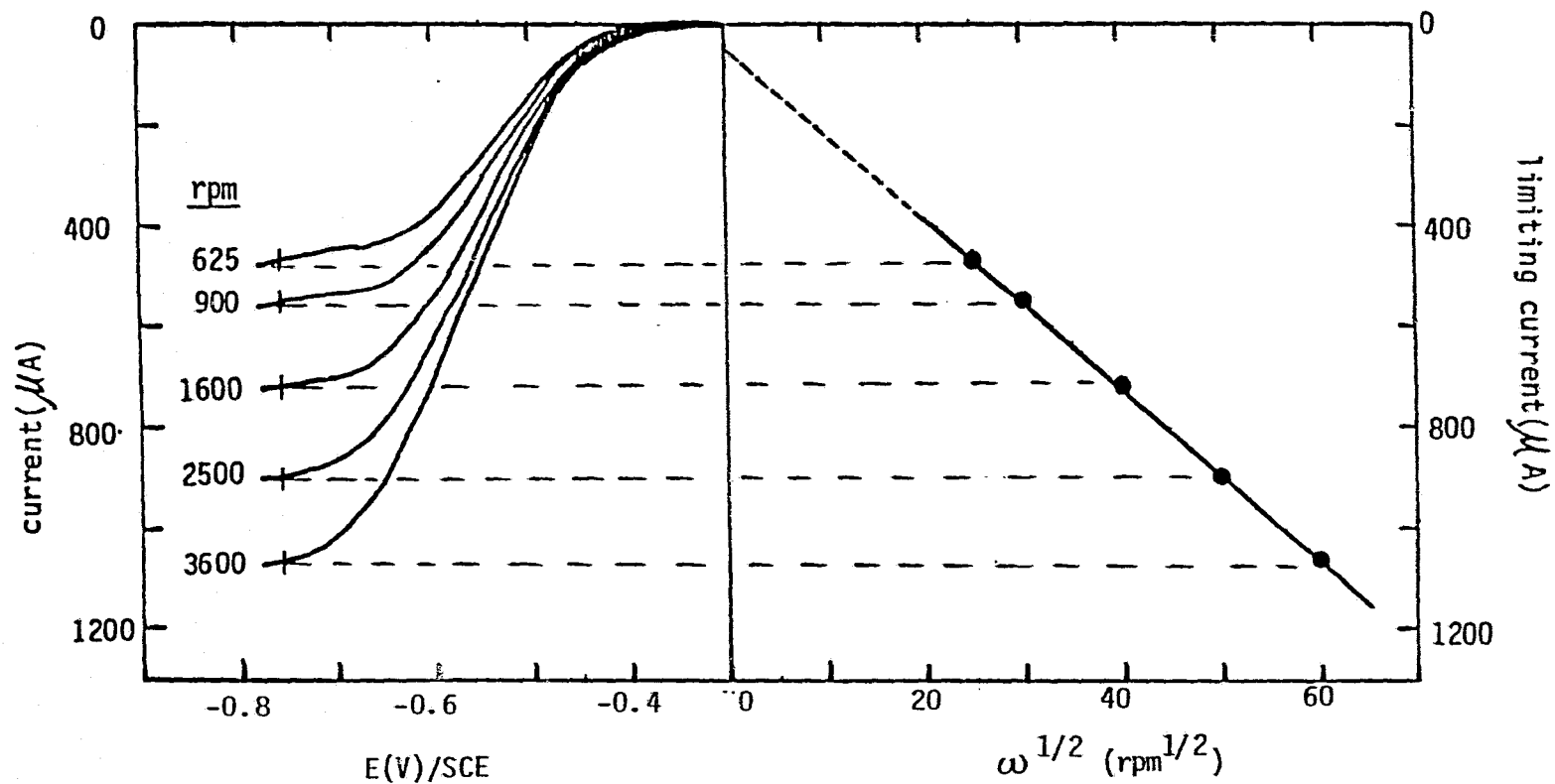
Figure 10: Polarization curves and corresponding i_L vs. $\omega^{1/2}$ plot for 7 mM $CrCl_3$ reduction on silver plated gold disk electrode. Electrolyte: 0.1 M $NaClO_4$ and 0.01 M $HClO_4$. Sweep rate: 10 mV/s. Electrode area: 0.196 cm^2.

Figure 11: $1/i$ vs. $1/\omega^{1/2}$ plots for $CrCl_3$ reduction on silver plated gold electrode. Data taken from Fig. 10.

Figure 12: Tafel plots for 7 mM $CrCl_3$ reduction on
silver(o) and silver plated gold(●) rotating
disk electrodes. Electrode areas: 0.196 cm^2.
Rotation rate: 900 rpm; i_L= 0.63 mA.
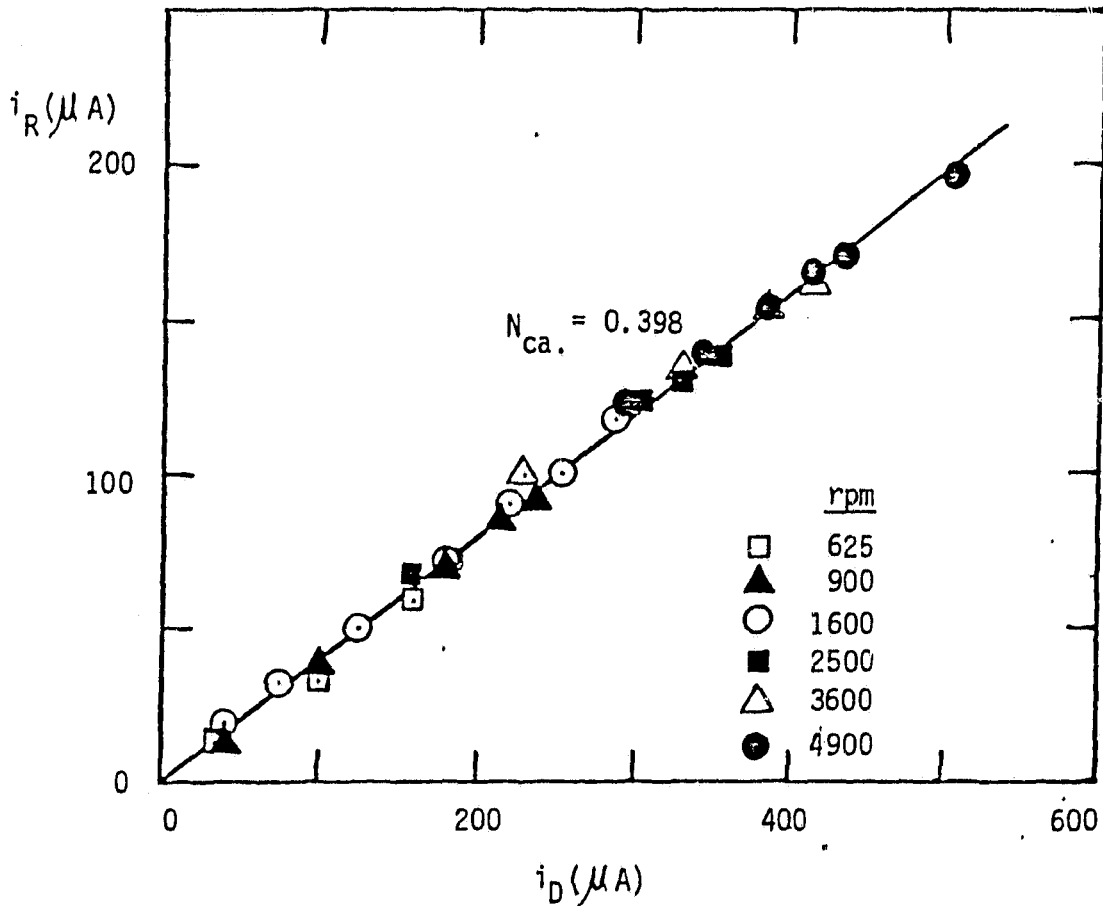
Figure 13: i_D vs. i_R plot for gold disk and gold ring electrode.
Solution: 0.1 M $NaClO_4$, 0.01 M $HClO_4$ and 3.2 mM $Fe(ClO_4)_3$.
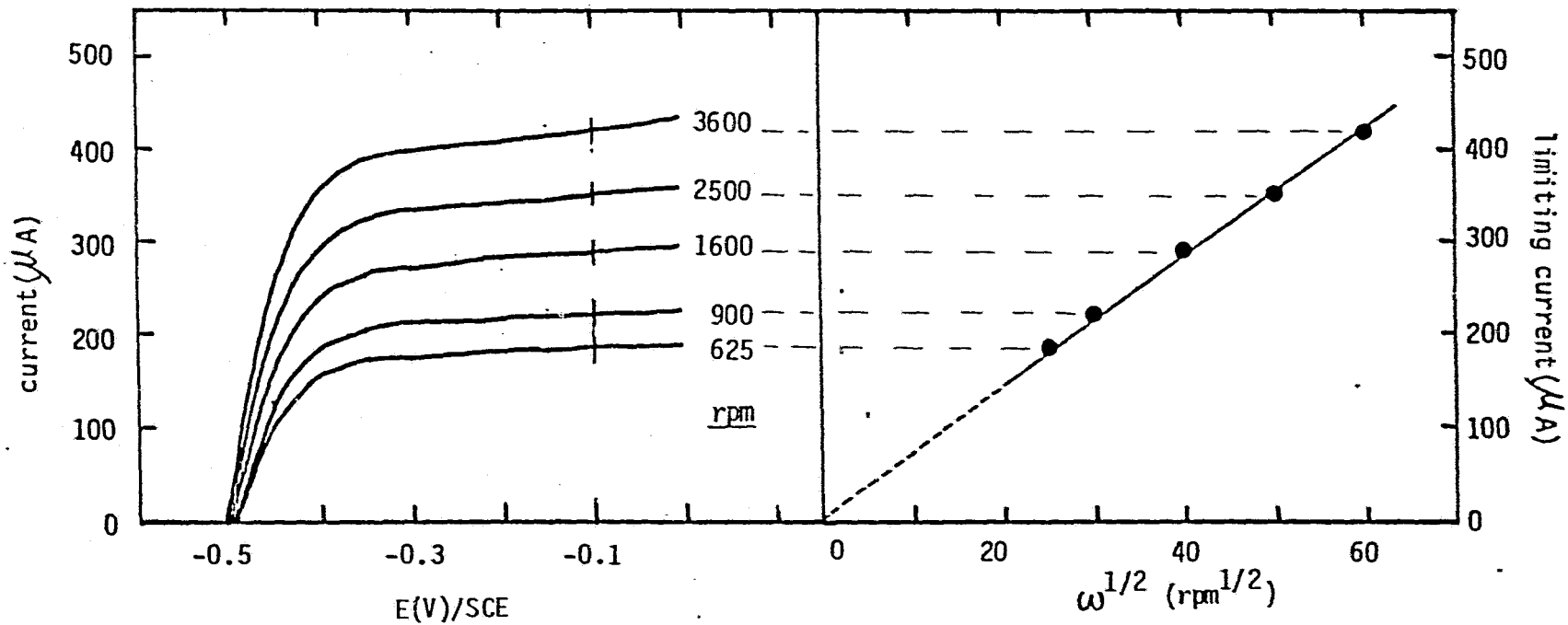
Figure 14: Ring polarization curves and corresponding i_L vs. $\omega^{1/2}$ plot for Cr(II) oxidation on silver plated gold ring electrode with $E_{disk}= -0.7$ V vs. SCE. Solution: 0.1 M NaClO$_4$, 0.01 M HClO$_4$ and 7 mM CrCl$_3$. Sweep rate: 10 mV/s. Electrode area: 0.196 cm^2.
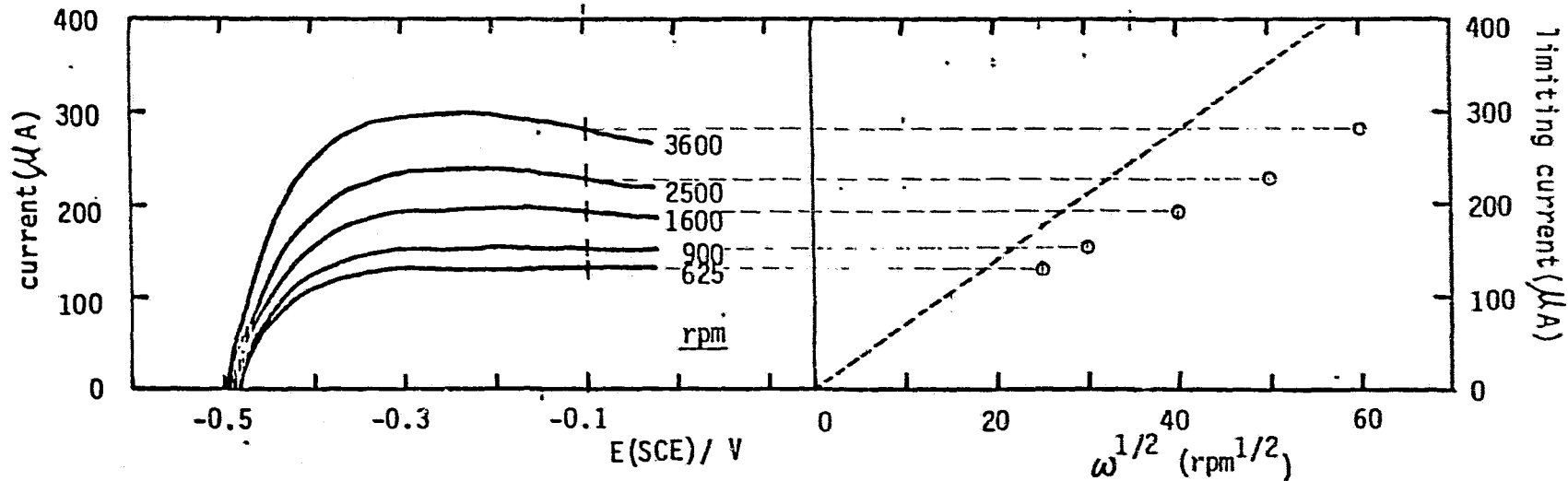
Figure 15: Ring polarization curves and corresponding i_L vs. $\omega^{1/2}$ plot for Cr(II) oxidation on gold ring electrode with silver plated gold disk electrode under potentiostatic condition, E_{disk}= -0.7V vs. SCE. Solution: 0.1 M NaClO$_4$, 0.01 M HClO$_4$ and 7 mM CrCl$_3$. Sweep rate: 10 mV/s. Electrode area: 0.196 cm^2.
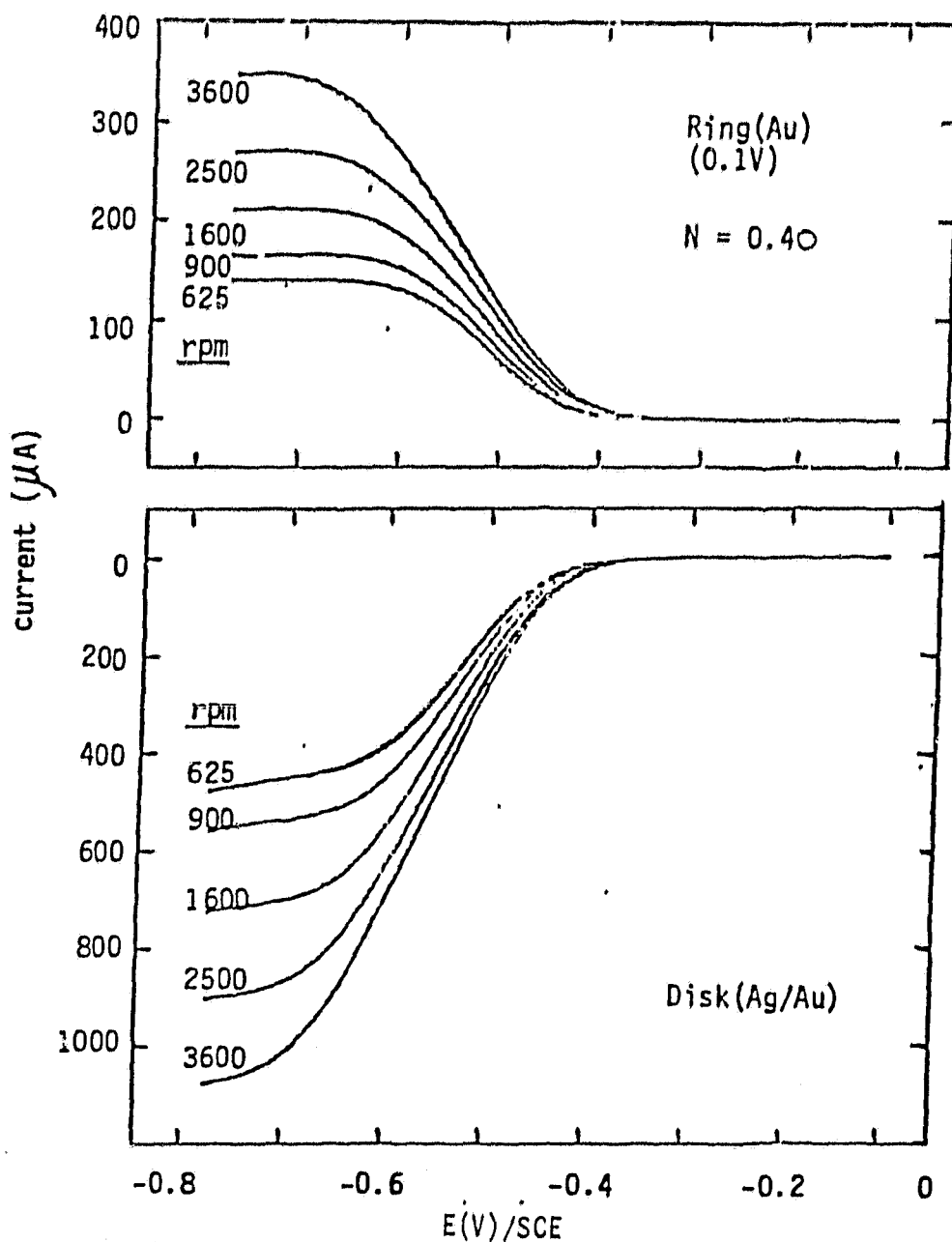
Figure 16: Polarization curves for $CrCl_3$ reduction on silver plated gold disk electrode. Solution: 0.1 M $NaClO_4$, 0.01 M $HClO_4$ and 7 mM $CrCl_3$. Electrode area: 0.196 cm^2. Sweep rate: 10 mV/s.
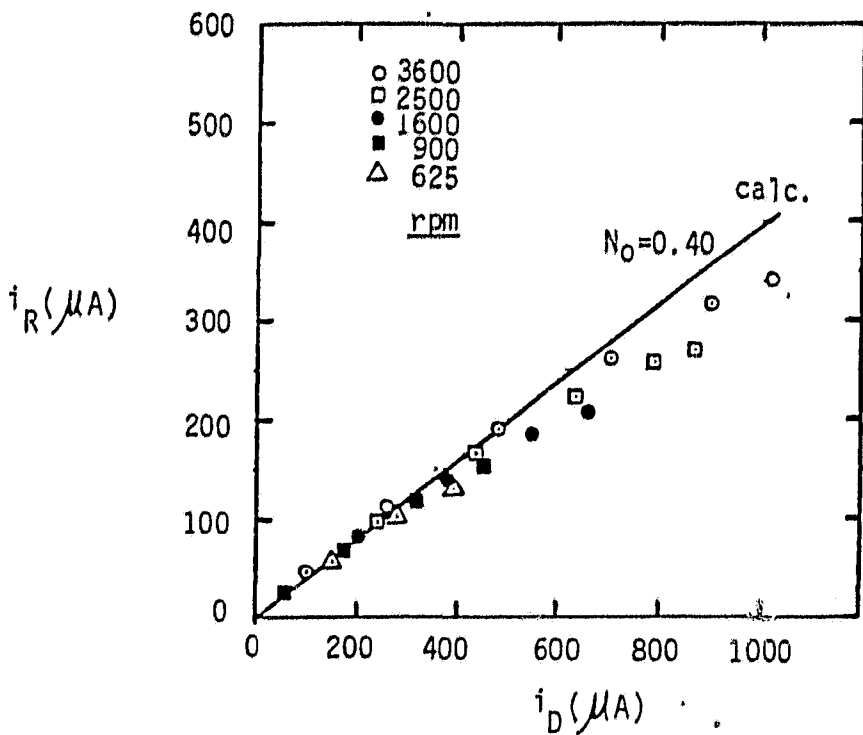
Figure 17: i_D vs. i_R plot for silver plated gold disk
and ring electrode. Data obtained from Fig. 16.
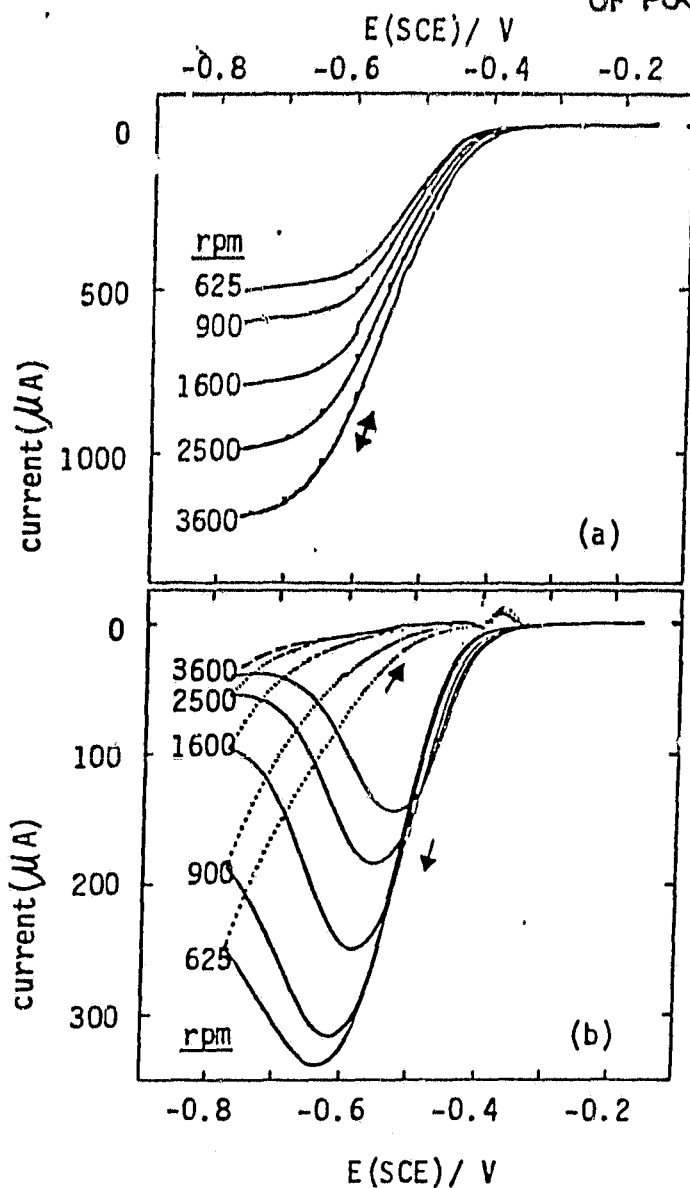
Figure 18: Polarization curves for 7 mM $CrCl_3$ reduction on silver disk electrode with (b) and without (a) 3.81×10^{-6} M PbC. Electrolyte: 0.1 M $NaClO_4$ and 0.01 M $HClO_4$. Sweep rate: 10 mV/s. Electrode area: 0.196 cm^2.

ORIGINAL PAGE IS
OF POOR QUALITY
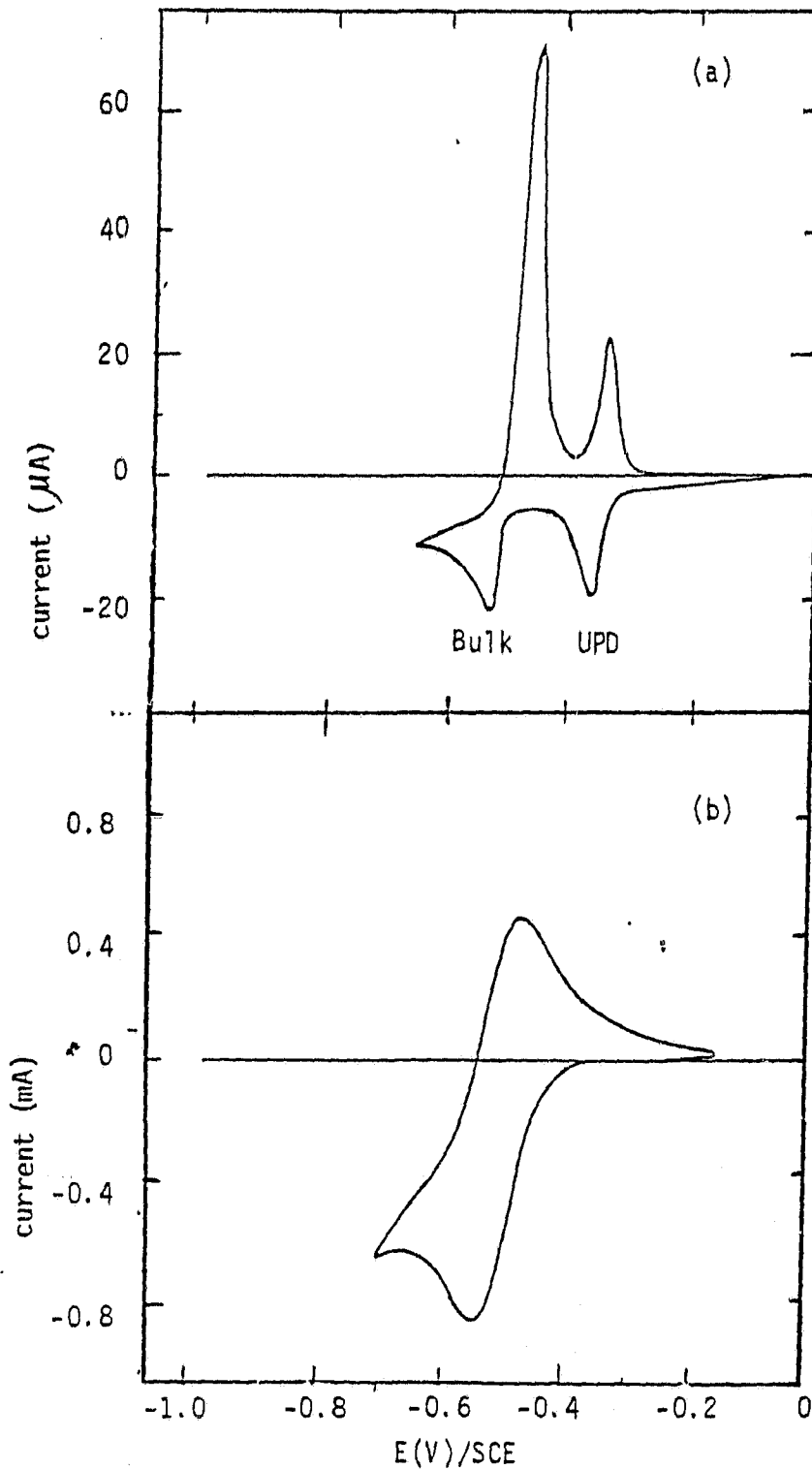
Figure 19: a) Cyclic voltammogram for lead UPD and bulk deposition on
silver electrode(A= 0.196 cm^2). Electrolyte: 0.1 M NaClO$_4$,
0.01 M HClO$_4$ and 3.8 mM NaCl, 3.8 10^{-4}M PbO (pH=2.1). b).
Cyclic voltammogram for 7 mM CrCl$_3$ reduction on silver electrode
in 0.1 M NaClO$_4$ and 0.01 M HClO$_4$.
Electrode area: 0.196 cm^2. Sweep rate: 10 mV/s.
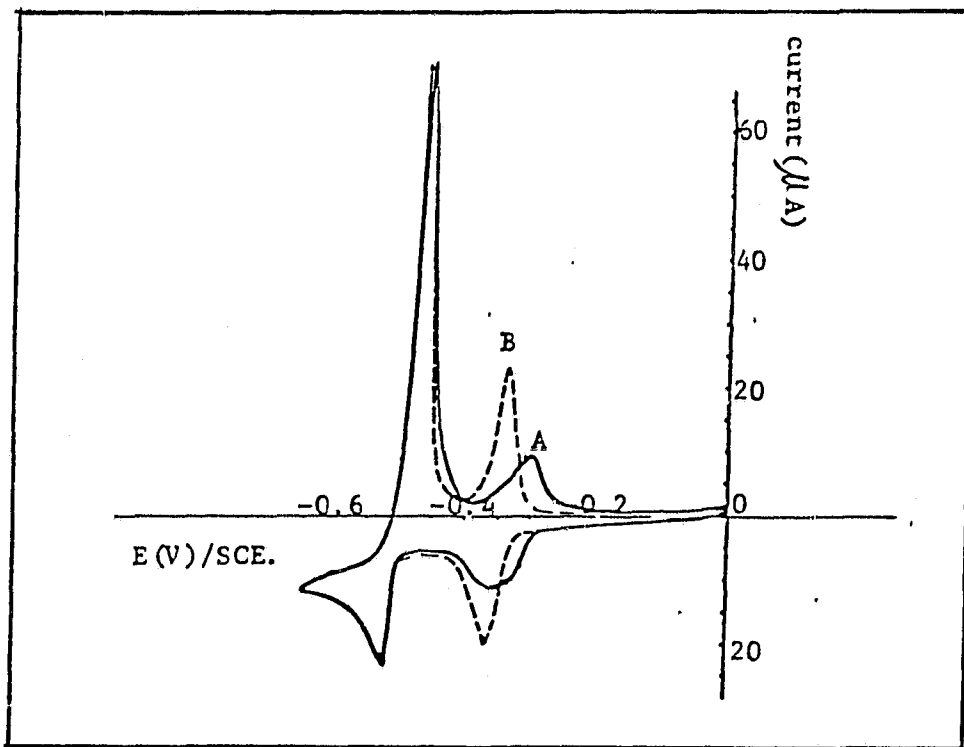
Figure 20: Platting and stripping of Pb(II) on silver disk
electrode. Electrolyte: 0.1 M NaClO$_4$ and HClO$_4$ (pH=
2.2), 3.8×10^{-4} M PbO. Sweep rate: 10 mV/s. Electrode
area: 0.2 cm^2. (A). no NaCl (B). 3.8 mM NaCl.
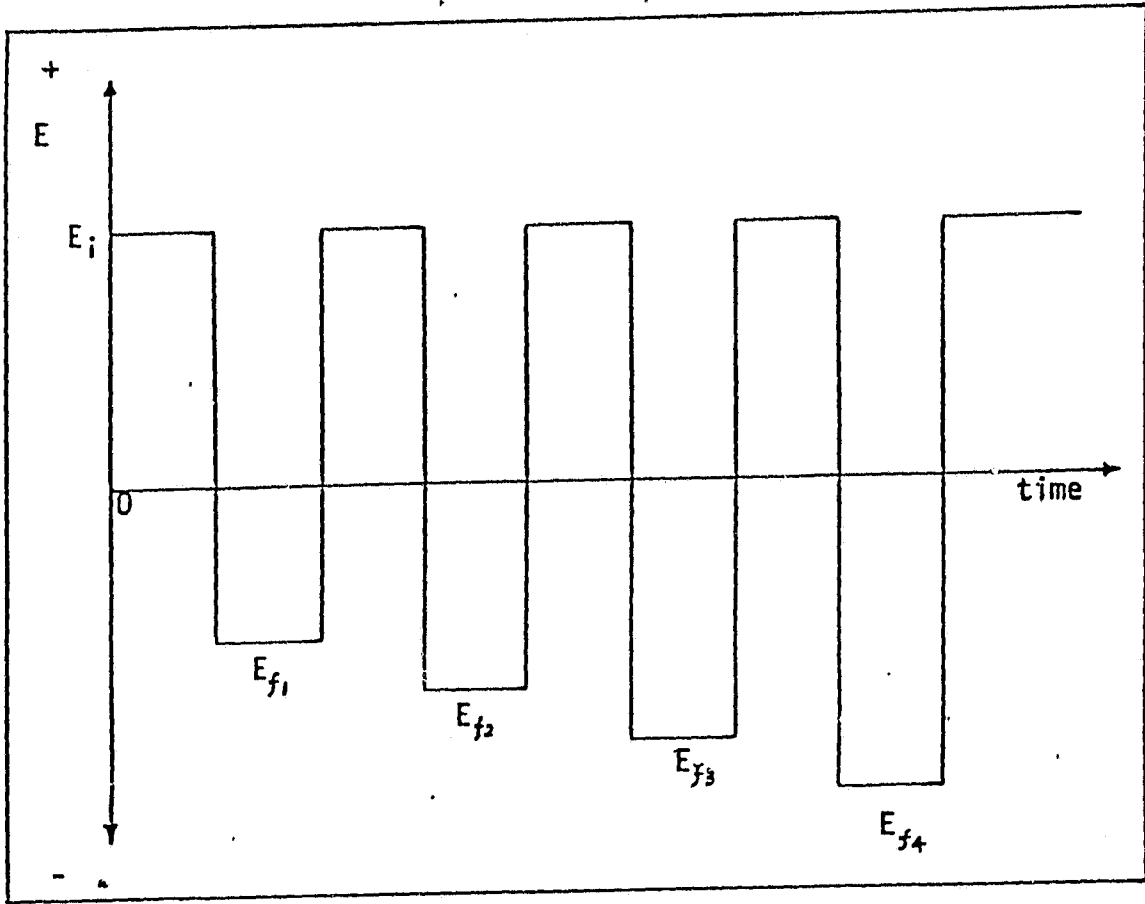
Figure 21: Potential step waveforms applied in a series of experiments.
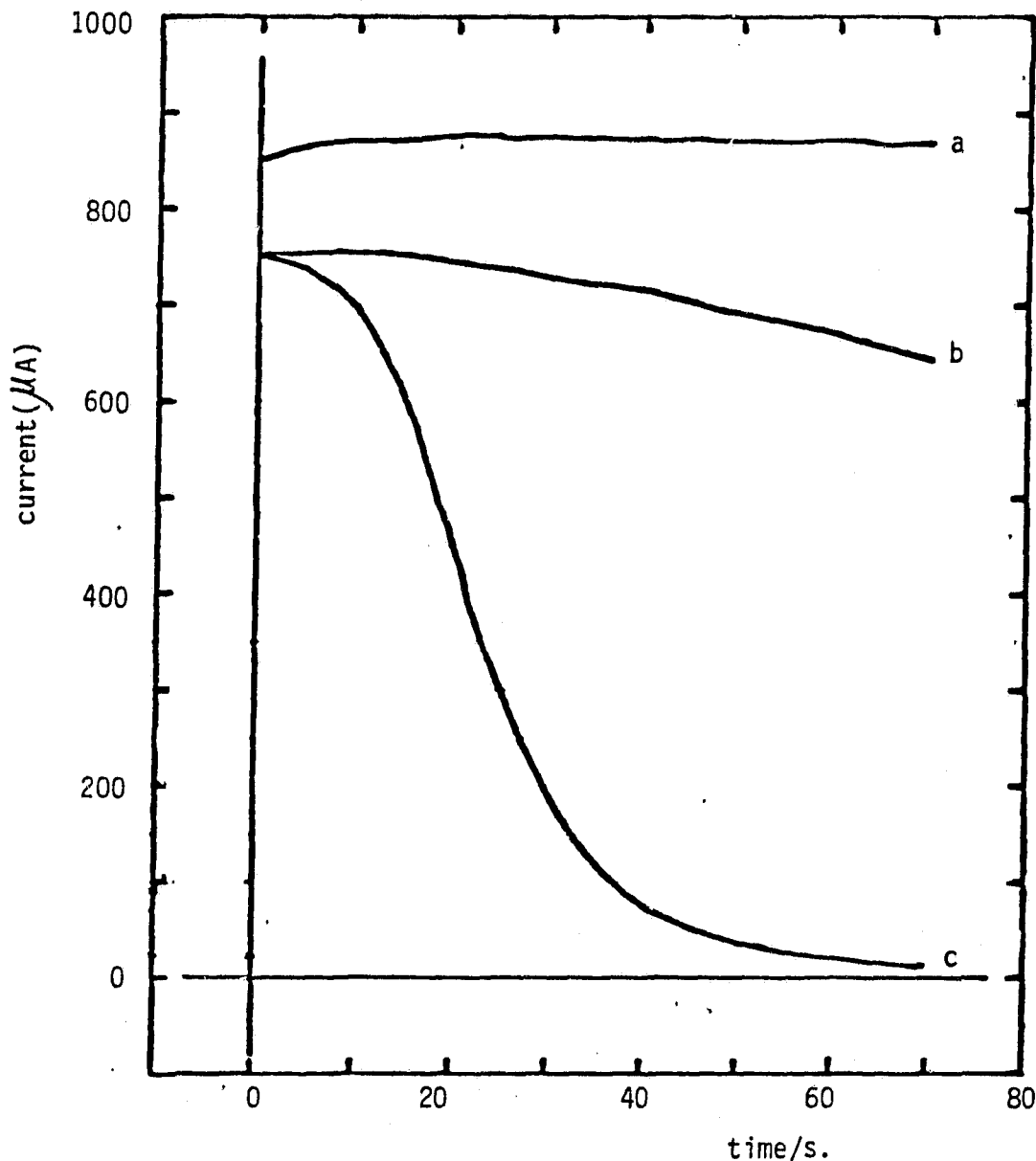
Figure 22: Current vs. time curves for simultaneous lead
deposition and $CrCl_3$ reduction on rotating silver
disk electrode upon potential step from -0.1V into
-0.7V(SCE). Solution: 7 mM $CrCl_3$ in 0.1 M $NaClO_4$,
0.01 M $HClO_4$ and (a). no PbO, (b).3.57×10^{-7}M PbO
and (c). 3.81×10^{-6}M PbO. Rotation rate: 1600 rpm.
Electrode area: 0.196 cm^2.

Figure 23: Current vs. time curves for simultaneous lead deposition and CrCl$_3$ reduction on rotating silver disk electrode upon potential step from -0.1V into (a). -0.4V (b). -0.5V (c). -0.6V (d). -0.7V (SCE). Solution: 7 mM CrCl$_3$ in 0.1 M NaClO$_4$, 0.01 M HClO$_4$ and 3.81$\cdot$10^{-6}M PbO. Rotation rate: 1600 rpm. Electrode area: 0.196 cm^2.
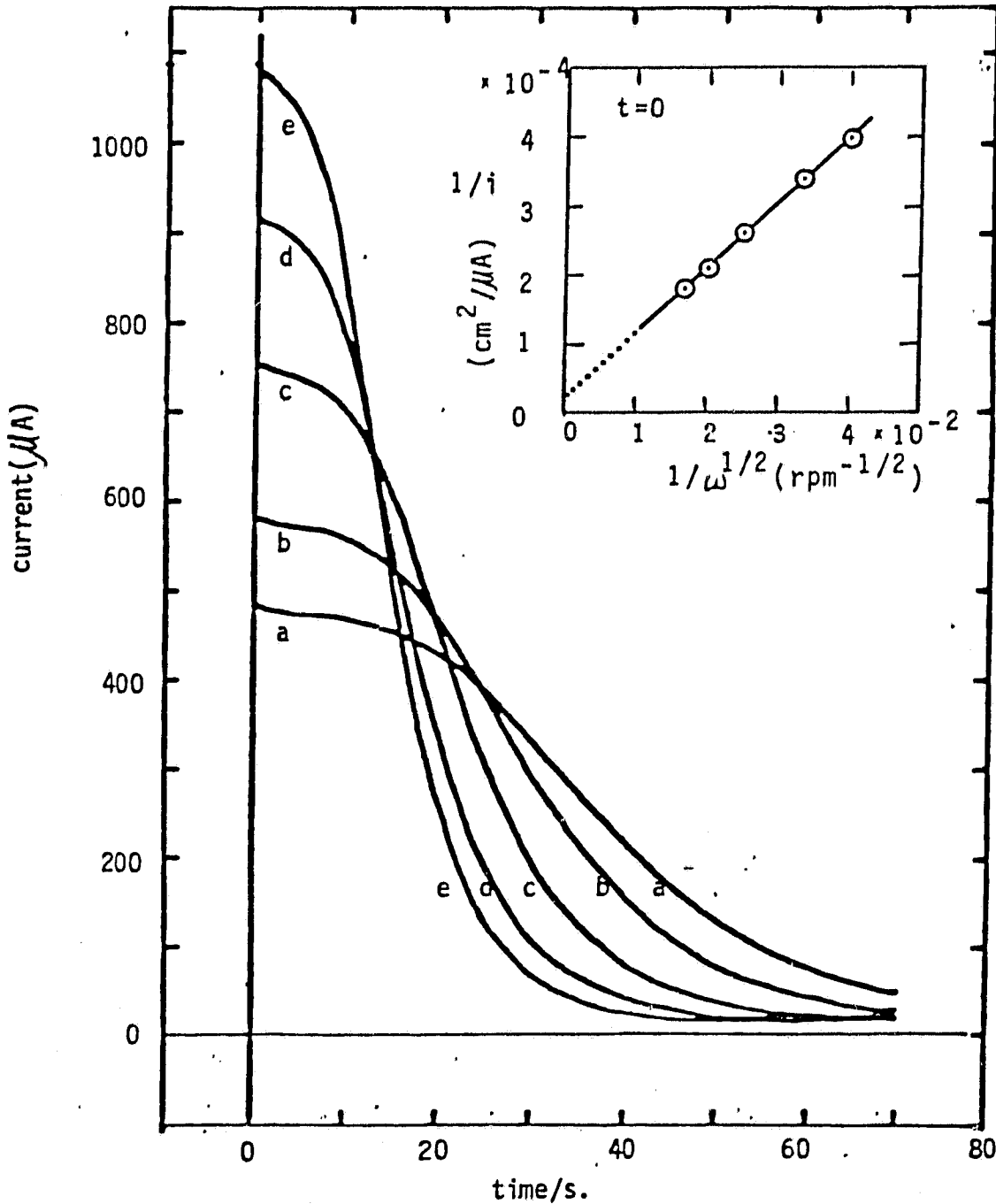
Figure 24: Current vs. time curves for simultaneous lead deposition and CrCl$_3$ reduction on rotating silver disk electrode upon potential step from -0.1V into -0.7V (SCE). Solution: 7 mM CrCl$_3$ in 0:1 M NaClO$_4$, 0.01 M HClO$_4$ and 3.81·10^{-6}M PbO. Electrode area: 0.196 cm^2. Rotation rate: a) 625rpm, b) 900 rpm, c) 1600 rpm, d) 2500 rpm and e) 3600 rpm.

Figure 25: Current vs. time curves for rotating silver disk electrode in a solution containing 0.1 M $NaClO_4$, 0.01 M $HClO_4$ and 7.4×10^{-6}M PbO upon potential step from -0.1 V into indicated potential. Electrode area: 0.196 cm^2. Rotation rate: 900 rpm.
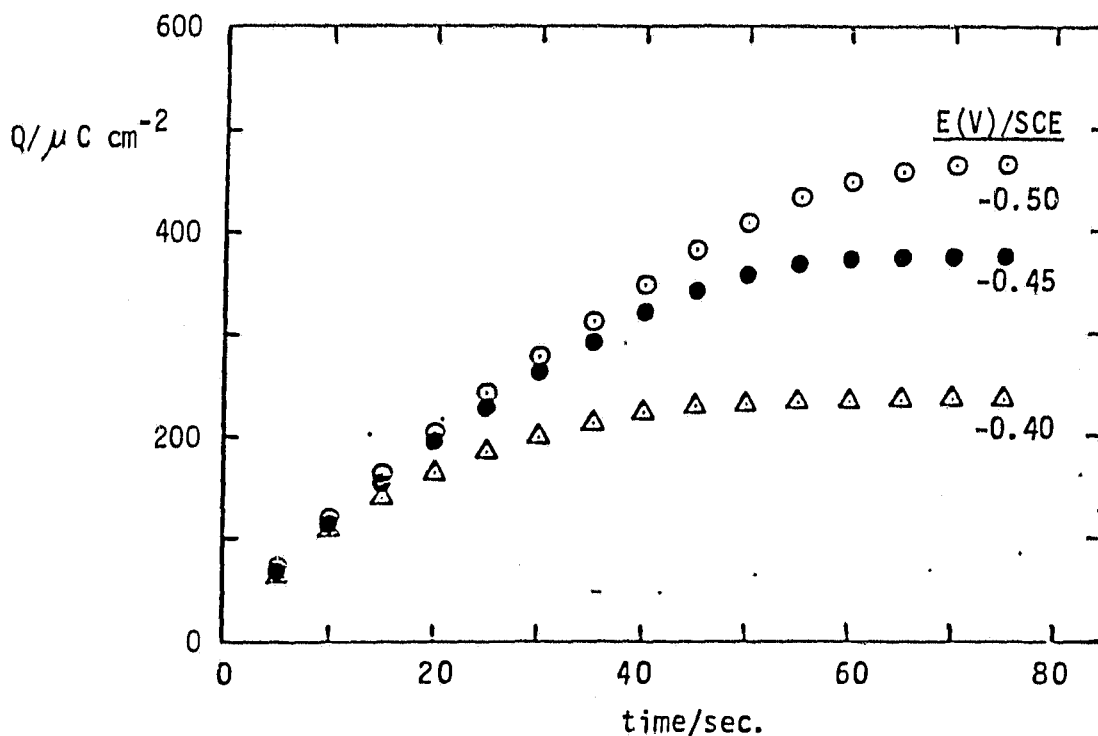
Figure 26: Charge of lead UPD vs..time curves constructed from
Fig. 25. [PbO]= 7.4 $\times 10^{-6}$M. Rotation rate: 900rpm.
Electrode area: 0.196cm^2.
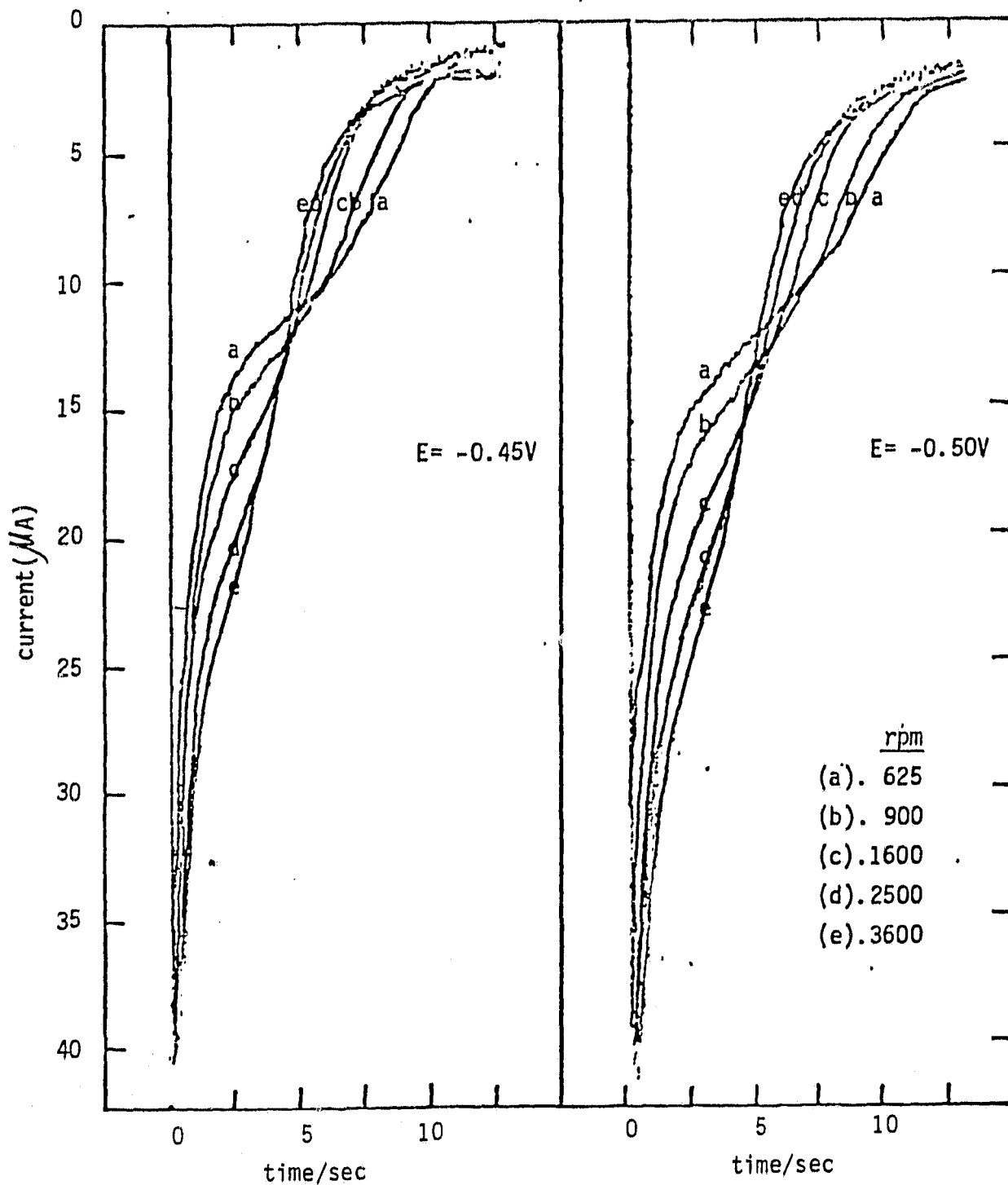
Figure 27: Current vs. time curves for rotating silver disk electrode in a solution containing 0.1 M $NaClO_4$, 0.01 M $HClO_4$ and 7.7×10^{-5} M PbO upon potential step from 0.0V into indicated potential. Electrode area: 0.196 cm^2.
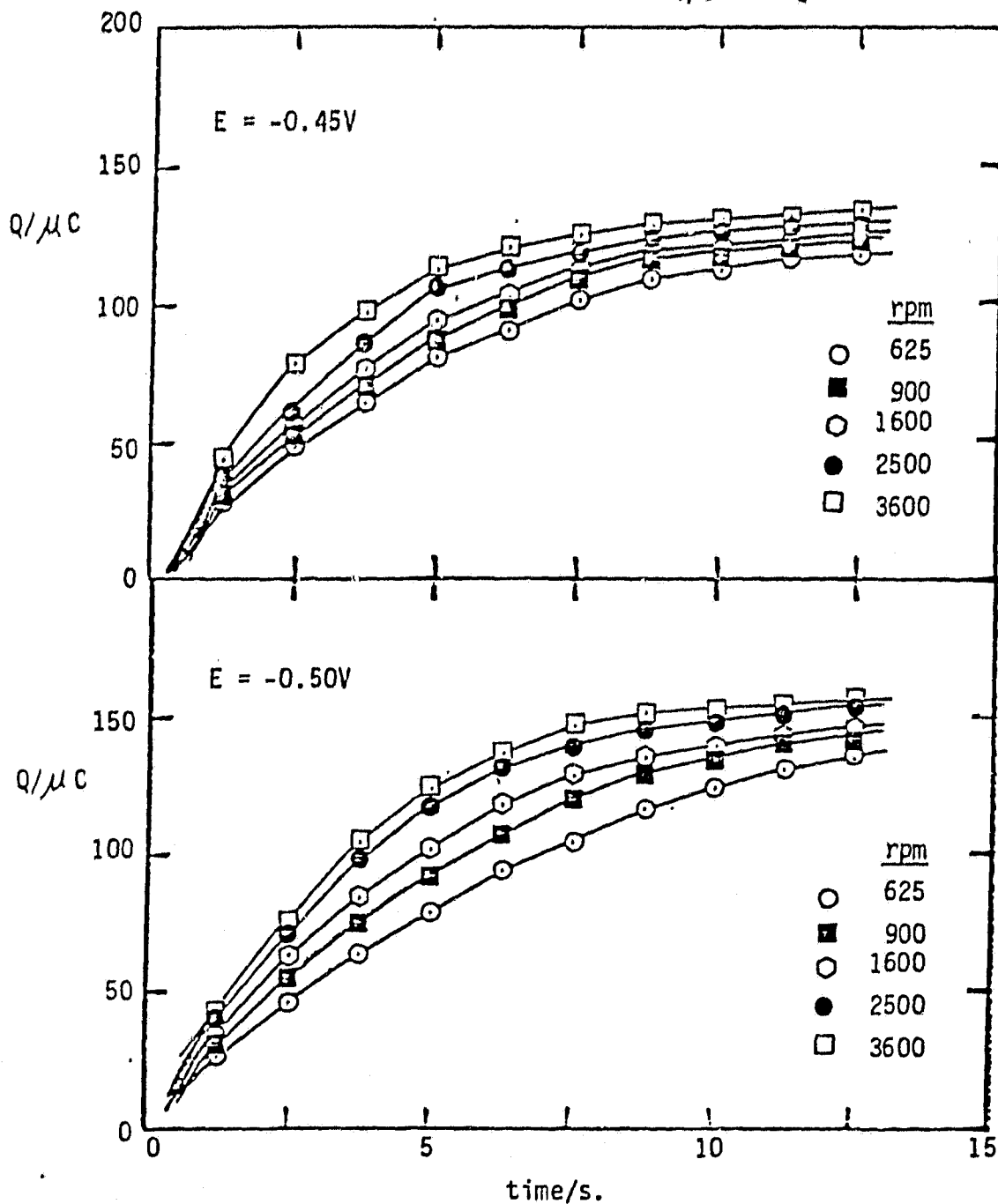
Figure 28: Charge of lead UPD vs. time curves for different
rotation rate. Data obtained from Fig.27.
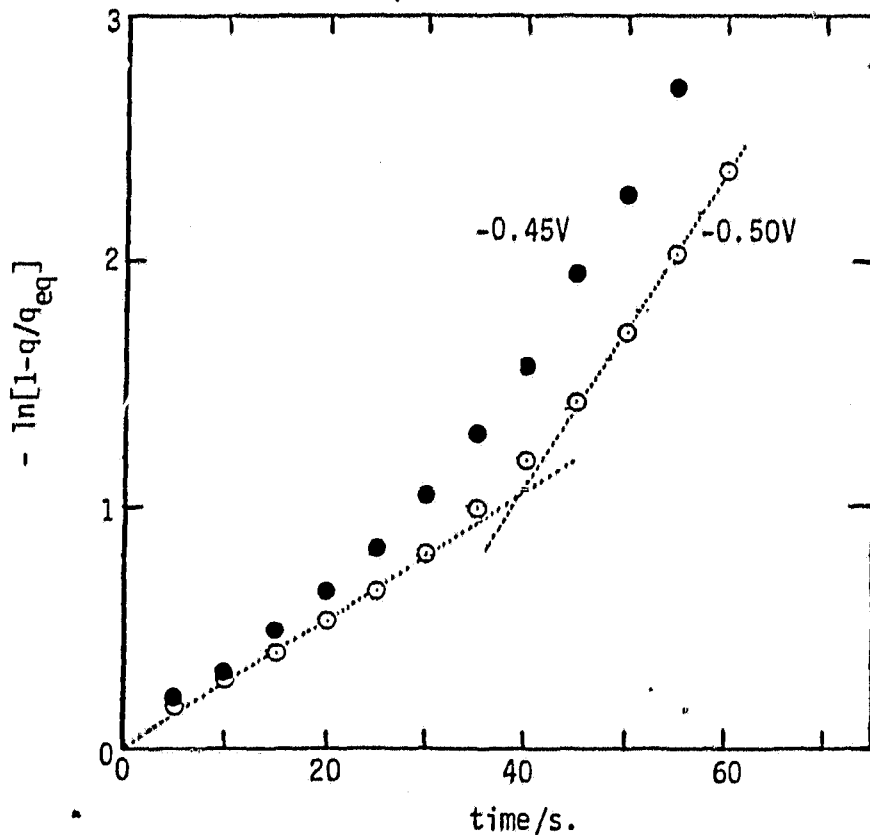
Figure 29: $-\ln[1-q/q_{eq}]$ vs. time curves for lead
UPD under rotation. Data obtained from
Fig. 25. Rotation rate: 900 rpm.

$q_{eq}(-0.45V) = 105.5 \mu C$; $q_{eq}(-0.50V) = 136 \mu C$.
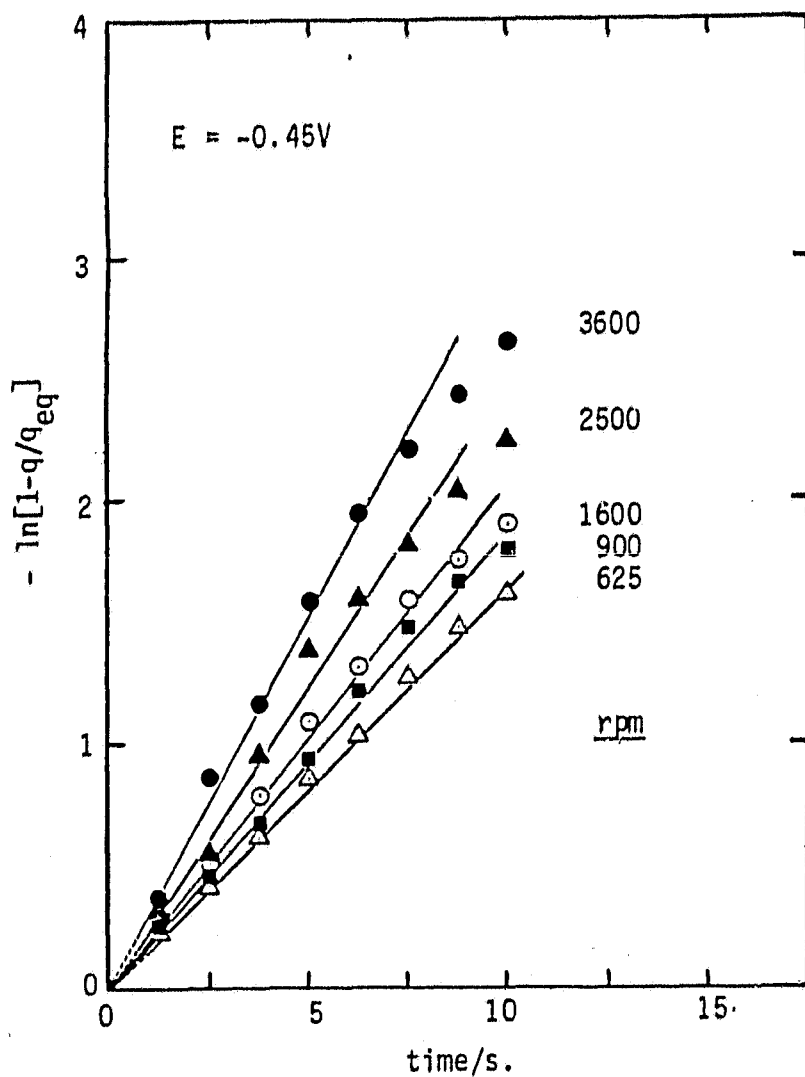
Figure 30: $- \ln[1-q/q_{eq}]$ vs. time curves for lead UPD
under rotation. Data obtained from Fig. 27.
$q_{eq}(-0.45V) = 140 \mu C$.
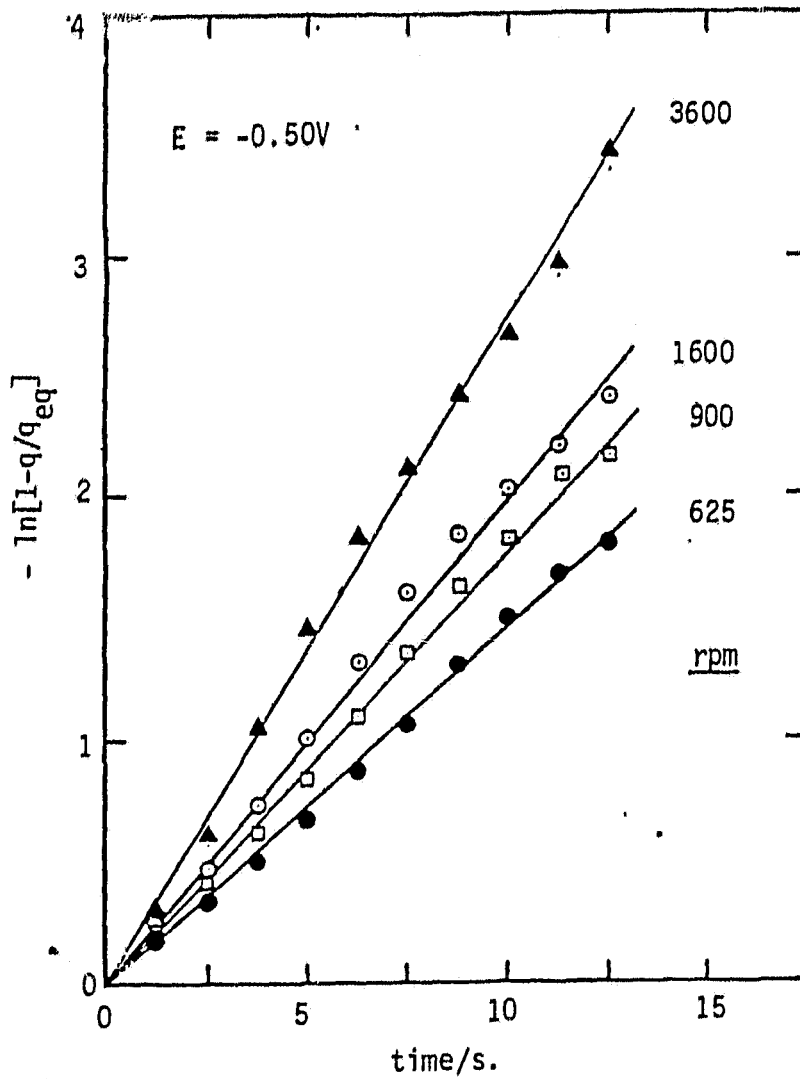
Figure 31: $-\ln[1-q/q_{eq}]$ vs. time curves for lead UPD under rotation. Data obtained from Fig. 27. $q_{eq}(-0.50V) = 160\,\mu C.$
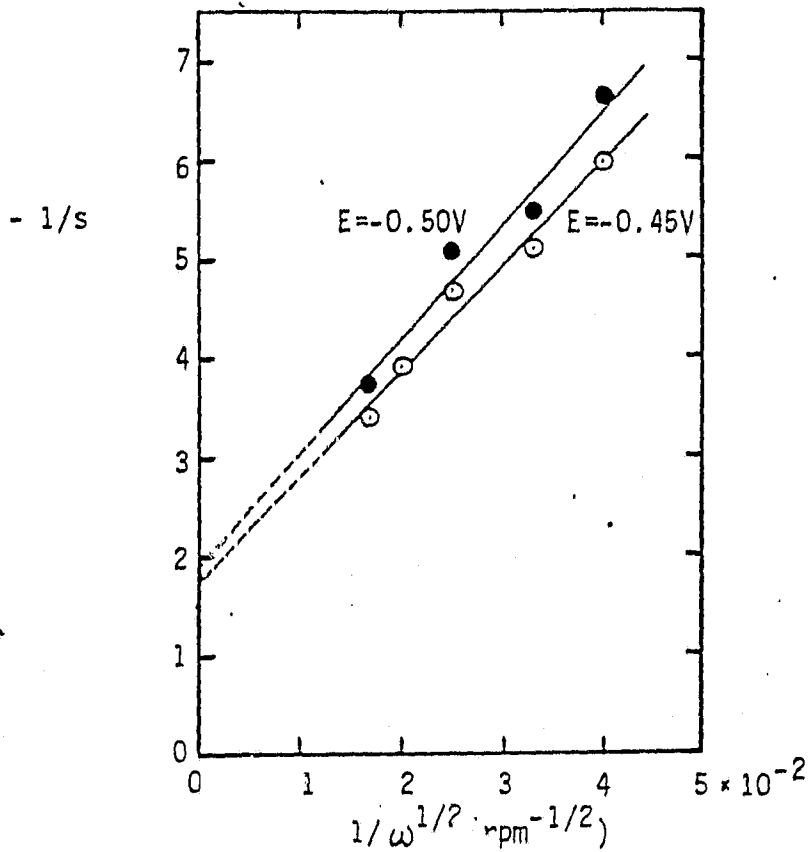
Figure 32: -1/s vs. $1/\omega^{1/2}$ plots constructed
from the data of Fig.30 and 31.
s is the slope of ~ $\ln[1-q/q_{eq}]$ vs.
time plot.
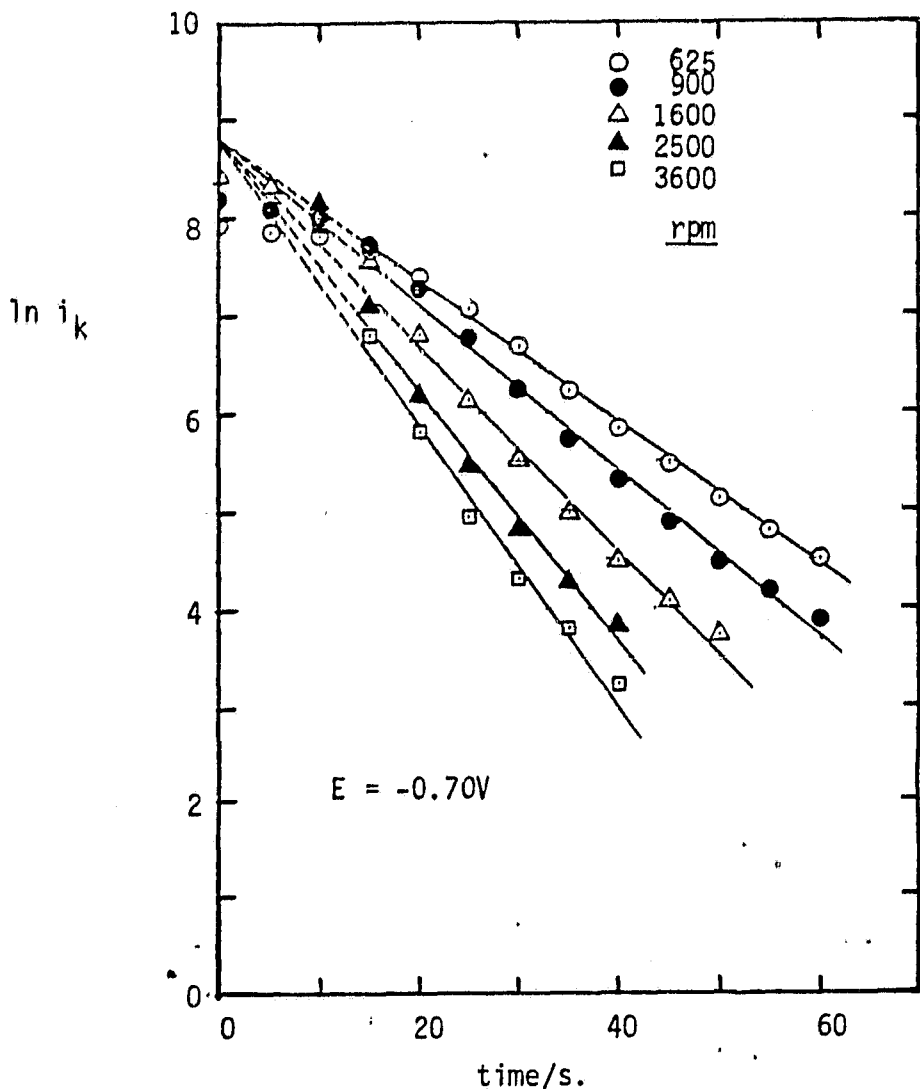
Figure 33: ln i_k vs. time curves for simultaneous lead
deposition and $CrCl_3$ reduction on silver.
Data obtained from Fig.24 with current be
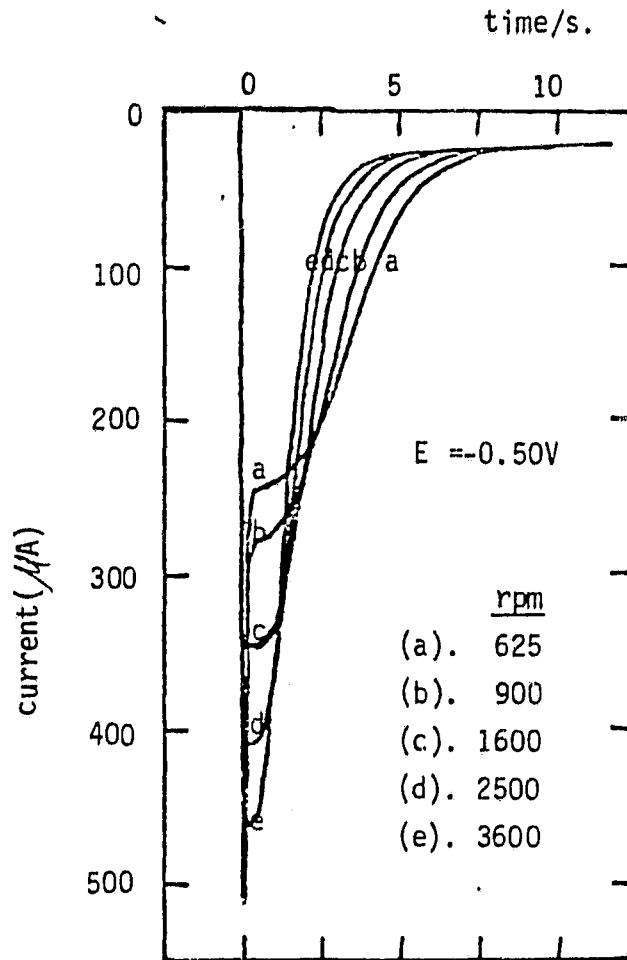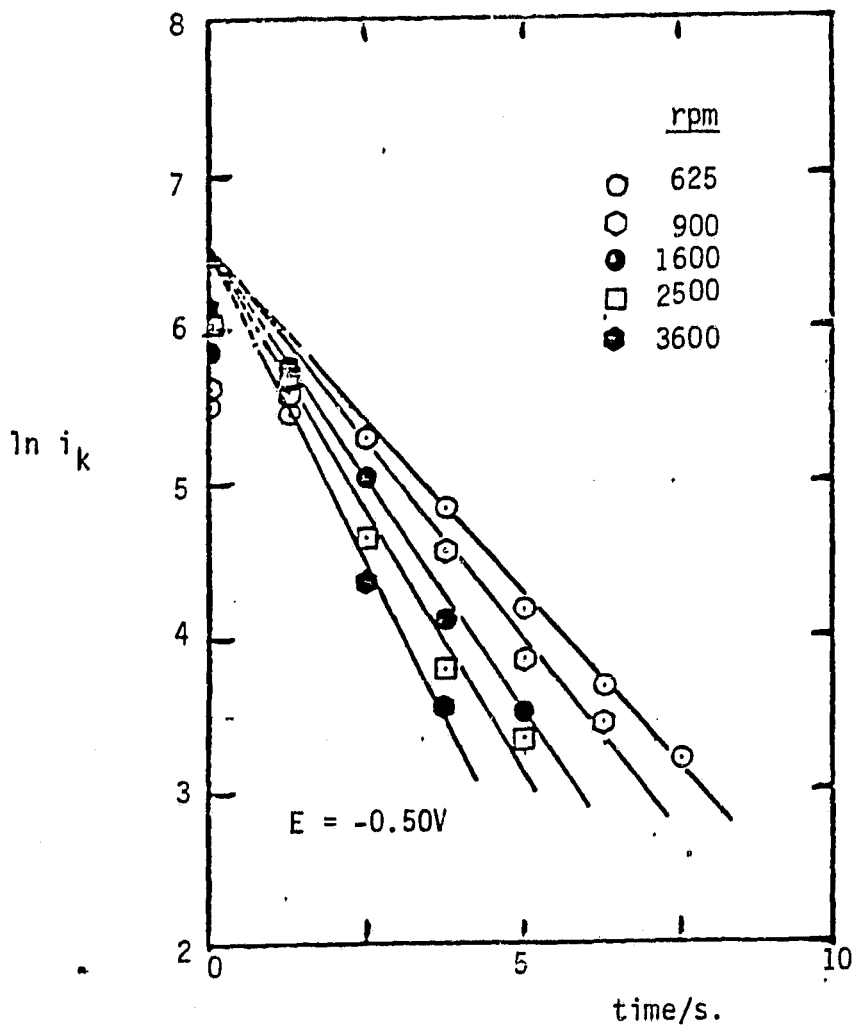corrected by:

$$i_k = \frac{1}{\frac{1}{i} - \frac{1}{i_d}}$$

Figure 34: Current vs time curves for $CrCl_3$ reduction in solution containing PbO on silver disk electrode upon potential step from 0.0V into -0.50V. Solution: 0.1 M $NaClO_4$, 0.01 M $HClO_4$, 7 mM $CrCl_3$ and 7.7×10^{-5} M PbO. Electrode area: 0.196 cm^2.

Figure 35: ln i_k vs. time curves for simultaneous lead
deposition and $CrCl_3$ reduction on silver.
Data obtained from Fig. 34 with current be
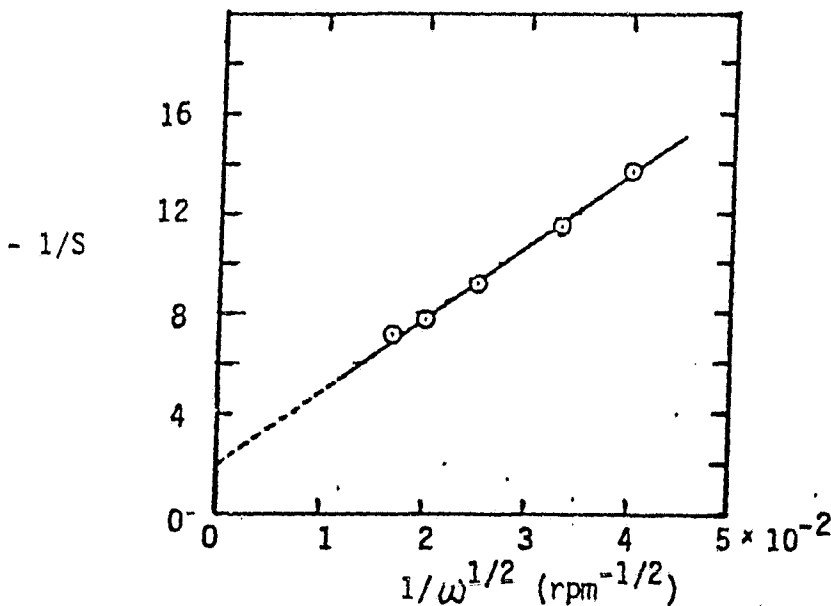corrected by:
$$i_k = \frac{1}{\frac{1}{i} - \frac{1}{i_d}}$$

Figure 36: -1/s vs. $1/\omega^{1/2}$ plot constructed from the data of Fig. 33. s is the slope of $\ln i_k$ vs. time plot.
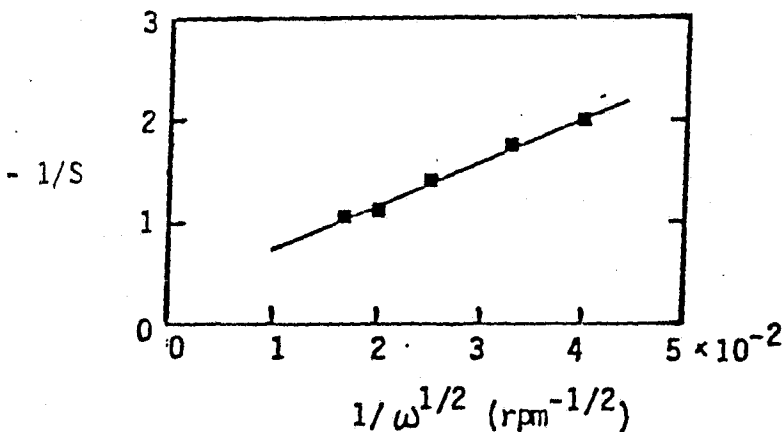

Figure 37: -1/s vs $1/\omega^{1/2}$ plot constructed from the data of Fig. 35. s is the slope of $\ln i_k$ vs. time plot.